The Journal of Chemical Physics

Current density functional framework for spin–orbit coupling

Cite as: J. Chem. Phys. **157**, 204102 (2022); https://doi.org/10.1063/5.0122394
Submitted: 24 August 2022 • Accepted: 04 November 2022 • Accepted Manuscript Online: 07 November 2022 • Published Online: 22 November 2022

Christof Holzer, Yannick J. Franzke and Ansgar Pausch

The Journal of Chemical Physics ARTICLE scitation.org/journal/jcp

Current density functional framework for spin–orbit coupling

Cite as: J. Chem. Phys. 157, 204102 (2022); doi: 10.1063/5.0122394
Submitted: 24 August 2022 • Accepted: 4 November 2022 •
Published Online: 22 November 2022

Christof Holzer,[1,a)] Yannick J. Franzke,[2,a)] and Ansgar Pausch[3]

AFFILIATIONS

[1] Institute of Theoretical Solid State Physics, Karlsruhe Institute of Technology (KIT), Wolfgang-Gaede-Straße 1, 76131 Karlsruhe, Germany
[2] Fachbereich Chemie, Philipps-Universität Marburg, Hans-Meerwein-Straße 4, 35032 Marburg, Germany
[3] Institute of Physical Chemistry, Karlsruhe Institute of Technology (KIT), Fritz-Haber-Weg 2, 76131 Karlsruhe, Germany

Note: This paper is part of the 2022 JCP Emerging Investigators Special Collection.
[a)]**Authors to whom correspondence should be addressed:** christof.holzer@kit.edu and yannick.franzke@chemie.uni-marburg.de

ABSTRACT

Relativistic two-component density functional calculations are carried out in a non-collinear formalism to describe spin–orbit interactions, where the exchange–correlation functional is constructed as a generalization of the non-relativistic density functional approximation. Contrary to non-relativistic density functional theory (DFT), spin–orbit coupling, however, leads to a non-vanishing paramagnetic current density. Density functionals depending on the kinetic energy density, such as meta-generalized gradient approximations, should therefore be constructed in the framework of current DFT (CDFT). The latter has previously exclusively been used in the regime of strong magnetic fields. Herein, we present a consistent CDFT approach for relativistic DFT, including spin–orbit coupling. Furthermore, we assess the importance of the current density terms for ground-state energies, excitation energies, nuclear magnetic resonance shielding, and spin–spin coupling constants, as well as hyperfine coupling constants, Δg-shifts, and the nuclear quadrupole interaction tensor in electron paramagnetic resonance (EPR) spectroscopy. The most notable changes are found for EPR properties. The impact of the current-dependent terms rises with the number of unpaired electrons, and consequently, the EPR properties are more sensitive toward CDFT. Considerable changes are observed for the strongly constrained and appropriately normed functionals, as well as the B97M family and TASK. The current density terms are less important when exact exchange is incorporated. At the same time, the current-dependent kernel ensures the stability of response calculations in all cases. We, therefore, strongly recommend to use the framework of CDFT for self-consistent spin–orbit calculations.

I. INTRODUCTION

A theoretical framework for physical and chemical properties of heavy elements necessitates a consideration of quantum mechanics and the inclusion of special relativity.[1–9] The so-called relativistic effects refer to the difference between the results obtained from the Schrödinger equation and its relativistic counterparts, such as the Dirac equation or approximations thereof.[10–15] These relativistic effects are commonly partitioned into a scalar-relativistic contribution, associated with the spatial contraction of the electron density, and spin–orbit interaction, which describes the energetic splitting of the atomic p, d, and f states. The latter leads to a breakdown of the spin symmetry and necessitates a complex two-component (2c) or four-component (4c) formalism when treated self-consistently. Due to the increased computational costs of a relativistic framework, mid-scale or large-scale calculations are typically performed with density functional theory (DFT) methods. This is usually done in a non-collinear formalism[16–32] using the total particle density matrix and the spin magnetization vector. The expression of the exchange–correlation functional itself is taken from the non-relativistic limit and evaluated with the so-called spin-up and spin-down quantities similar to the one-component unrestricted Kohn–Sham (UKS) formalism. Relativistic corrections to the functional expression were shown to be marginal.[33–38] In

recent years, such spin–orbit density functional methods have become available in many quantum chemistry software suites.[39–47] The two-component and four-component generalization of the local spin density approximation (LSDA) and generalized gradient approximation (GGA) is straightforward. However, a sophisticated generalization of meta-generalized gradient approximations (*meta*-GGAs) and most local hybrid functionals (LHFs)[48–53] requires additional considerations.

In detail, spin–orbit coupling is a form of magnetic induction.[2,54,55] This is also illustrated in Refs. 4, 56, and 57 with the introduction of spin–orbit coupling in the spirit of an internal magnetic field. Here, the interaction of the electron spin with the field of a charge in relative motion leads to magnetic induction. This effect induces a paramagnetic current density $\vec{j}_\mathrm{p}$ of the one-electron spinor functions $\{\varphi_j\}$. Here, the orbital contribution is defined as

$$\vec{j}_{\mathrm{p},0} = -\frac{\mathrm{i}}{2}\sum_j \left(\varphi_j^\dagger \vec{\nabla}\varphi_j - \left[\vec{\nabla}\varphi_j\right]^\dagger \varphi_j\right), \tag{1}$$

and the spin counterparts using the Pauli matrices σ_u follow as

$$\vec{j}_{\mathrm{p},u} = -\frac{\mathrm{i}}{2}\sum_j \left(\varphi_j^\dagger \sigma_u \vec{\nabla}\varphi_j - \left[\vec{\nabla}\varphi_j\right]^\dagger \sigma_u \varphi_j\right) \quad \forall u \in \{x,y,z\}. \tag{2}$$

In two-component calculations, the paramagnetic current density of the ground state does not generally vanish.[53,55,58,59] In other words, current-carrying states[60–63] are observed. As noted in Ref. 64, for Kramers-restricted systems, the total or particle contribution of the paramagnetic current density vanishes, but the spin counterparts do not. Consequently, the kinetic energy density τ of *meta*-GGAs needs to be generalized and the most suited ansatz to generalize τ is to consider the paramagnetic current density $\vec{j}_\mathrm{p}$ itself. Here, $\vec{j}_\mathrm{p}$ does not depend explicitly on the specific magnetic perturbation.[65–67] Thus, the generalized kinetic energy density reads

$$\tilde{\tau} = \tau - \frac{\vec{j}_\mathrm{p}^{\,2}}{2\rho} \quad \text{with } \tau = \sum_j \left(\hat{\vec{p}}\,\varphi_j\right)^\dagger \left(\hat{\vec{p}}\varphi_j\right), \tag{3}$$

with the electron density ρ and the momentum operator $\hat{\vec{p}}$. We note in passing that $\tilde{\tau}$ originally arises for the Fermi curvature[65] or the time-dependent electron localization function[68] of the Schrödinger equation. Using Eq. (3), the density functional approximations do not only depend on the electron density ρ and its derivatives but also on the current density $\vec{j}_\mathrm{p}$. Accordingly, functionals need to be constructed in the framework of current density functional theory (CDFT).[58,69–83]

Currently, CDFT is well established for molecular calculations in strong magnetic fields,[58,76,80–83] i.e., formulations and implementations for ground-state energies, gradients, and excitation energies have been presented. However, we are not aware of a detailed study on spin–orbit coupling within the framework of CDFT. In this work, CDFT will therefore be applied to the self-consistent treatment of spin–orbit interaction, and we study its impact on ground-state energies, excitation energies, and magnetic resonance parameters, where the spin–orbit perturbation is introduced by either spin–orbit effective core potentials[1] (ECPs) or the one-electron exact two-component (X2C) Hamiltonian.[84–94] Besides calculations in strong magnetic fields and CDFT, the generalized kinetic energy density was applied to linear response theory for time-dependent density functional theory (TD-DFT),[95,96] electron paramagnetic resonance (EPR) spectra,[97,98] nuclear magnetic resonance (NMR) properties,[97–102] and magnetizabilities.[100] In all these approaches, the paramagnetic current density of the ground state was assumed to vanish. Yet, the non-zero response of the current density already substantially affects the results in spin–orbit perturbation approaches of the g-tensor for transition-metal complexes with a doublet ground state.[98] Therefore, a generalization to a self-consistent treatment of spin–orbit coupling, which also includes the current density in the calculation of the ground-state density matrix, seems promising—especially for chemical systems with more than one unpaired electron.

II. THEORY

A. Exchange–correlation potential in current density functional theory

In a non-collinear two-component framework,[16,17] we define the spin magnetization vector as

$$\vec{m} = \sum_j \varphi_j^\dagger \vec{\sigma} \varphi_j, \tag{4}$$

with the one-electron spinor functions φ_j and the vector $\vec{\sigma}$ consisting of the (2×2) Pauli spin matrices

$$\sigma_x = \begin{pmatrix} 0 & 1 \\ 1 & 0 \end{pmatrix}, \quad \sigma_y = \begin{pmatrix} 0 & -\mathrm{i} \\ \mathrm{i} & 0 \end{pmatrix}, \quad \sigma_z = \begin{pmatrix} 1 & 0 \\ 0 & -1 \end{pmatrix}. \tag{5}$$

The total particle density ρ and the non-collinear spin density s read

$$\rho = \sum_j \varphi_j^\dagger \varphi_j, \tag{6}$$

$$s = (\vec{m}\cdot\vec{m})^{1/2} = \sqrt{m_x^2 + m_y^2 + m_z^2}. \tag{7}$$

The 2c evaluation of the exchange–correlation (XC) potential is based on a non-relativistic density functional approximation being generalized with the spin-up and spin-down quantities, e.g.,

$$\rho_\uparrow = (\rho + s)/2, \tag{8}$$

$$\rho_\downarrow = (\rho - s)/2. \tag{9}$$

Therefore, an unrestricted Kohn–Sham implementation can be straightforwardly generalized to the two-component methodology. The interested reader is referred to Refs. 16, 17, and 19 for more details. Furthermore, the exchange–correlation energy E^XC is based on a non-relativistic functional expression g^XC. Thus, the

exchange–correlation energy is a function of the density, its gradient, and the (generalized) kinetic energy density,

$$E^{\mathrm{XC}} = \int f^{\mathrm{XC}}[\rho_{\uparrow,\downarrow}(\vec{r}), \gamma_{\uparrow\uparrow,\uparrow\downarrow,\downarrow\downarrow}(\vec{r}), \tau_{\uparrow,\downarrow}(\vec{r}), j_{\mathrm{p};\uparrow,\downarrow}(\vec{r})]\, d^3r = \int g^{\mathrm{XC}}[\rho_{\uparrow,\downarrow}(\vec{r}), \gamma_{\uparrow\uparrow,\uparrow\downarrow,\downarrow\downarrow}(\vec{r}), \tilde{\tau}_{\uparrow,\downarrow}(\vec{r})]\, d^3r. \tag{10}$$

Here, we used the minimal substitution $\tau \to \tilde{\tau}$ for the CDFT methodology, leading from the explicitly current dependent f^{XC} to g^{XC}. Furthermore, the auxiliary variable $\gamma_{\sigma\sigma'} = \frac{1}{4}(\vec{\nabla}\rho_\sigma)\cdot(\vec{\nabla}\rho_{\sigma'})$ with $\sigma, \sigma' \in \{\uparrow,\downarrow\}$ has been introduced. Introducing the basis set approximation with the set of real atom-centered functions $\{\chi_\mu\}$, the XC expressions are evaluated based on the four complex density matrices $\mathbf{M}$,

$$M^0_{\mu\nu} = \frac{1}{2}\left[P^{\alpha\alpha}_{\mu\nu} + P^{\beta\beta}_{\mu\nu}\right], \tag{11}$$

$$M^x_{\mu\nu} = \frac{1}{2}\left[P^{\alpha\beta}_{\mu\nu} + P^{\beta\alpha}_{\mu\nu}\right], \tag{12}$$

$$M^y_{\mu\nu} = \frac{\mathrm{i}}{2}\left[P^{\alpha\beta}_{\mu\nu} - P^{\beta\alpha}_{\mu\nu}\right], \tag{13}$$

$$M^z_{\mu\nu} = \frac{1}{2}\left[P^{\alpha\alpha}_{\mu\nu} - P^{\beta\beta}_{\mu\nu}\right]. \tag{14}$$

Equations (11)–(14) arise from applying the 2 × 2 Pauli-spin matrices and the 2 × 2 unit matrix σ_0 on the full 2c density matrix $P_{\mu\nu} = \sum_i C^\mu_i C^{\nu*}_i$ with an additional prefactor of 0.5 for the (anti-)symmetrization. C^μ_i are the respective complex 2c Kohn–Sham spinor coefficients. Furthermore, $P^{\alpha\alpha}_{\mu\nu} = \sum_i C^\mu_{i,\alpha} C^{\nu*}_{i,\alpha}$ denotes the corresponding sub-block of the full density matrix. The remaining density matrices $P^{\alpha\beta}_{\mu\nu}$ and $P^{\beta\beta}_{\mu\nu}$ can be obtained accordingly by replacing one or both coefficients $C^\mu_{i,\alpha}$ by $C^\mu_{i,\beta}$. The density ρ, gradient of the density $\vec{\nabla}\rho$, and the kinetic energy density τ accordingly arise solely from the symmetric parts of Eqs. (11)–(14). The symmetric parts are $\mathrm{Re}(\mathbf{P}^{\alpha\alpha}) + \mathrm{Re}(\mathbf{P}^{\beta\beta})$, $\mathrm{Re}(\mathbf{P}^{\alpha\beta}) + \mathrm{Re}(\mathbf{P}^{\beta\alpha})$, $\mathrm{Im}(\mathbf{P}^{\alpha\beta}) - \mathrm{Im}(\mathbf{P}^{\beta\alpha})$, and $\mathrm{Re}(\mathbf{P}^{\alpha\alpha}) - \mathrm{Re}(\mathbf{P}^{\beta\beta})$. On the contrary, the paramagnetic current density is an anti-symmetric quantity, arising from the complimentary anti-symmetric parts, i.e., $\mathrm{Im}(\mathbf{P}^{\alpha\alpha}) + \mathrm{Im}(\mathbf{P}^{\beta\beta})$, $\mathrm{Im}(\mathbf{P}^{\alpha\beta}) + \mathrm{Im}(\mathbf{P}^{\beta\alpha})$, $\mathrm{Re}(\mathbf{P}^{\alpha\beta}) - \mathrm{Re}(\mathbf{P}^{\beta\alpha})$, and $\mathrm{Im}(\mathbf{P}^{\alpha\alpha}) - \mathrm{Im}(\mathbf{P}^{\beta\beta})$.

The derivatives of the XC energy needed for the construction of the two-component Kohn–Sham equations can be written as

$$V^{\mathrm{XC}}(\vec{r}) = \frac{\delta E^{\mathrm{XC}}}{\delta\rho(\vec{r})}\sigma_0 + \sum_u \frac{\delta E^{\mathrm{XC}}}{\delta m_u(\vec{r})}\sigma_u = \frac{\delta E^{\mathrm{XC}}}{\delta\rho(\vec{r})}\sigma_0 + \sum_u \frac{\delta E^{\mathrm{XC}}}{\delta s(\vec{r})}\frac{m_u(\vec{r})\ \sigma_u}{s(\vec{r})} \tag{15}$$

for the density ρ and the non-collinear spin magnetizations m_u. ρ and m_u can be obtained from the symmetric (sy) parts of the density matrices $\mathbf{M}^u$ as

$$\rho(\vec{r}) = \sum_{\mu\nu} M^{0,\mathrm{sy}}_{\mu,\nu}[\chi_\mu(\vec{r})\chi_\nu(\vec{r})], \tag{16}$$

$$m_u(\vec{r}) = \sum_{\mu\nu} M^{u,\mathrm{sy}}_{\mu,\nu}[\chi_\mu(\vec{r})\chi_\nu(\vec{r})]. \tag{17}$$

Note that the kinetic energy density and $\vec{j}_{\mathrm{p}}$ are implicit and not explicit functionals of the density as discussed in Ref. 83. For the purpose of an implementation, the XC potential in a matrix representation is required. Hence, the derivative is formed with respect to the density matrices instead of the particle density and the spin magnetization.[103] This directly leads to the matrix expression of V^{XC}, i.e., $V^{\mathrm{XC}}_{\mu\nu} = \langle\chi_\mu|V^{\mathrm{XC}}(\vec{r})|\chi_\nu\rangle$. Further necessary ingredients, i.e., the gradient of the density $\vec{\nabla}\rho$, the kinetic energy density τ, and the paramagnetic current density $\vec{j}_{\mathrm{p}}$, can be obtained from $\mathbf{M}^m$ (with $m \in \{0,x,y,z\}$) as

$$\vec{\nabla}\rho_m(\vec{r}) = \sum_{\mu,\nu} M^{m,\mathrm{sy}}_{\mu\nu}\left[\vec{\nabla}\chi_\mu(\vec{r})\chi_\nu(\vec{r}) + \chi_\mu(\vec{r})\vec{\nabla}\chi_\nu(\vec{r})\right], \tag{18}$$

$$\tau_m(\vec{r}) = \frac{1}{2}\sum_{\mu,\nu} M^{m,\mathrm{sy}}_{\mu\nu}\left[\vec{\nabla}\chi_\mu(\vec{r})\cdot\vec{\nabla}\chi_\nu(\vec{r})\right], \tag{19}$$

$$\vec{j}_{\mathrm{p},m}(\vec{r}) = -\frac{\mathrm{i}}{2}\sum_{\mu,\nu} M^{m,\mathrm{as}}_{\mu\nu}\left[\vec{\nabla}\chi_\mu(\vec{r})\chi_\nu(\vec{r}) - \chi_\mu(\vec{r})\vec{\nabla}\chi_\nu(\vec{r})\right]. \tag{20}$$

As the paramagnetic current density is an anti-symmetric (as) quantity, the implementation of the XC potential also requires a generalization of the code infrastructure. Thus, we need the same density matrices as for the evaluation of exact exchange, and the current density can lead to contributions even in a Kramers-restricted framework.[64]

The derivative of the XC energy with respect to one of the density matrices $\mathbf{M}$ can then be obtained using the chain rule accordingly as

$$\frac{\delta E^{\mathrm{XC}}}{\delta M^m_{\mu\nu}} = \int\left[\frac{\partial g^{\mathrm{XC}}}{\partial\rho(\vec{r})}\frac{\partial\rho(\vec{r})}{\partial M^m_{\mu\nu}} + \frac{\partial g^{\mathrm{XC}}}{\partial\vec{\nabla}\rho(\vec{r})}\frac{\partial\vec{\nabla}\rho(\vec{r})}{\partial M^m_{\mu\nu}} + \frac{\partial g^{\mathrm{XC}}}{\partial\tilde{\tau}(\vec{r})}\frac{\partial\tilde{\tau}(\vec{r})}{\partial M^m_{\mu\nu}}\right]\mathrm{d}^3r, \tag{21}$$

where the last term arises from the current-dependent *meta*-GGA ingredient $\tilde{\tau}$[83] and $m \in \{0,x,y,z\}$. By inserting Eq. (3), this term can be rewritten as

$$\frac{\partial\tilde{\tau}}{\partial M^m_{\mu\nu}} = \frac{\partial\tau}{\partial M^m_{\mu\nu}} - \frac{\vec{j}_{\mathrm{p}}}{\rho}\frac{\partial\vec{j}_{\mathrm{p}}}{\partial M^m_{\mu\nu}} + \frac{\vec{j}^{\,2}_{\mathrm{p}}}{2\rho^2}\frac{\partial\rho}{\partial M^m_{\mu\nu}}. \tag{22}$$

In contrast to CDFT for strong magnetic fields, the basis functions of a ground-state energy calculation are field-independent and real, i.e., no London atomic orbitals (LAOs) or gauge-including atomic orbitals (GIAOs) are employed.[104,105] Using the chain rule again, the needed derivatives of f^{XC} or g^{XC} can be recovered as

$$V^{\mathrm{XC}}_{\mu\nu,0} = \int \left[\frac{\partial g^{\mathrm{XC}}}{\partial \rho_\uparrow} + \frac{\vec{j}^{\,2}_{\mathrm{p},\uparrow}}{2\rho^2_\uparrow} \frac{\partial g^{\mathrm{XC}}}{\partial \tilde{\tau}_\uparrow} + \frac{\partial g^{\mathrm{XC}}}{\partial \rho_\downarrow} + \frac{\vec{j}^{\,2}_{\mathrm{p},\downarrow}}{2\rho^2_\downarrow} \frac{\partial g^{\mathrm{XC}}}{\partial \tilde{\tau}_\downarrow} \right] \chi_\mu(\vec{r})\ \chi_\nu(\vec{r})\ d^3r - \int \left[2\frac{\partial g^{\mathrm{XC}}}{\partial \gamma_{\uparrow\uparrow}} \vec{\nabla}\rho_\uparrow + 2\frac{\partial g^{\mathrm{XC}}}{\partial \gamma_{\downarrow\downarrow}} \vec{\nabla}\rho_\downarrow + \frac{\partial g^{\mathrm{XC}}}{\partial \gamma_{\uparrow\downarrow}} (\vec{\nabla}\rho_\uparrow + \vec{\nabla}\rho_\downarrow) \right]$$
$$\cdot \left[\{\vec{\nabla}\chi_\mu(\vec{r})\}\chi_\nu(\vec{r}) + \chi_\mu(\vec{r})\{\vec{\nabla}\chi_\nu(\vec{r})\} \right] d^3r + \int \frac{1}{2} \left[\frac{\partial g^{\mathrm{XC}}}{\partial \tilde{\tau}_\uparrow} + \frac{\partial g^{\mathrm{XC}}}{\partial \tilde{\tau}_\downarrow} \right] \left[\vec{\nabla}\chi_\mu(\vec{r}) \right] \cdot \left[\vec{\nabla}\chi_\nu(\vec{r}) \right] d^3r$$
$$+ \int \frac{\mathrm{i}}{2} \left[\frac{\vec{j}_{\mathrm{p},\uparrow}}{\rho_\uparrow} \frac{\partial g^{\mathrm{XC}}}{\partial \tilde{\tau}_\uparrow} + \frac{\vec{j}_{\mathrm{p},\downarrow}}{\rho_\downarrow} \frac{\partial g^{\mathrm{XC}}}{\partial \tilde{\tau}_\downarrow} \right] \left[\{\vec{\nabla}\chi_\mu(\vec{r})\}\chi_\nu(\vec{r}) - \chi_\mu(\vec{r})\{\vec{\nabla}\chi_\nu(\vec{r})\} \right] \mathrm{d}^3r \tag{23}$$

and

$$V^{\mathrm{XC}}_{\mu\nu,u} = \frac{m_u}{s} \int \left[\frac{\partial g^{\mathrm{XC}}}{\partial \rho_\uparrow} + \frac{\vec{j}^{\,2}_{\mathrm{p},\uparrow}}{2\rho^2_\uparrow} \frac{\partial g^{\mathrm{XC}}}{\partial \tilde{\tau}_\uparrow} - \frac{\partial g^{\mathrm{XC}}}{\partial \rho_\downarrow} - \frac{\vec{j}^{\,2}_{\mathrm{p},\downarrow}}{2\rho^2_\downarrow} \frac{\partial g^{\mathrm{XC}}}{\partial \tilde{\tau}_\downarrow} \right] \chi_\mu(\vec{r})\ \chi_\nu(\vec{r})\ d^3r - \int \left[2\frac{\partial g^{\mathrm{XC}}}{\partial \gamma_{\uparrow\uparrow}} \vec{\nabla}\rho_\uparrow - 2\frac{\partial g^{\mathrm{XC}}}{\partial \gamma_{\downarrow\downarrow}} \vec{\nabla}\rho_\downarrow - \frac{\partial g^{\mathrm{XC}}}{\partial \gamma_{\uparrow\downarrow}} (\vec{\nabla}\rho_\uparrow - \vec{\nabla}\rho_\downarrow) \right]$$
$$\cdot \left[\{\vec{\nabla}\chi_\mu(\vec{r})\}\chi_\nu(\vec{r}) + \chi_\mu(\vec{r})\{\vec{\nabla}\chi_\nu(\vec{r})\} \right] d^3r + \int \frac{1}{2} \left[\frac{\partial g^{\mathrm{XC}}}{\partial \tilde{\tau}_\uparrow} - \frac{\partial g^{\mathrm{XC}}}{\partial \tilde{\tau}_\downarrow} \right] \left[\vec{\nabla}\chi_\mu(\vec{r}) \right] \cdot \left[\vec{\nabla}\chi_\nu(\vec{r}) \right] d^3r$$
$$+ \int \frac{\mathrm{i}}{2} \left[\frac{\vec{j}_{\mathrm{p},\uparrow}}{\rho_\uparrow} \frac{\partial g^{\mathrm{XC}}}{\partial \tilde{\tau}_\uparrow} - \frac{\vec{j}_{\mathrm{p},\downarrow}}{\rho_\downarrow} \frac{\partial g^{\mathrm{XC}}}{\partial \tilde{\tau}_\downarrow} \right] \left[\{\vec{\nabla}\chi_\mu(\vec{r})\}\chi_\nu(\vec{r}) - \chi_\mu(\vec{r})\{\vec{\nabla}\chi_\nu(\vec{r})\} \right] \mathrm{d}^3r. \tag{24}$$

Note that the gradient or GGA part ($\vec{\nabla}\rho$ terms) is not affected by the inclusion of the current density. Equations (23) and (24) are evaluated numerically using a three-dimensional grid.[106–109] For updating the Kohn–Sham–Fock matrix, again the exchange–correlation potential is needed, similar to the density matrix, in the spinor blocks. The four blocks can be evaluated from Eqs. (23) and (24) as

$$V^{\mathrm{XC},\alpha\alpha}_{\mu\nu} = \frac{1}{2}(V^{\mathrm{XC}}_{\mu\nu,0} + V^{\mathrm{XC}}_{\mu\nu,z}), \tag{25}$$

$$V^{\mathrm{XC},\beta\beta}_{\mu\nu} = \frac{1}{2}(V^{\mathrm{XC}}_{\mu\nu,0} - V^{\mathrm{XC}}_{\mu\nu,z}), \tag{26}$$

$$V^{\mathrm{XC},\alpha\beta}_{\mu\nu} = \frac{1}{2}(V^{\mathrm{XC}}_{\mu\nu,x} - \mathrm{i}V^{\mathrm{XC}}_{\mu\nu,y}), \tag{27}$$

$$V^{\mathrm{XC},\beta\alpha}_{\mu\nu} = \frac{1}{2}(V^{\mathrm{XC}}_{\mu\nu,x} - \mathrm{i}V^{\mathrm{XC}}_{\mu\nu,y})^*. \tag{28}$$

To avoid numerical instabilities for a small spin density s, we use the collinear formalism with the z component for grid points with $\sqrt{m_x \cdot m_x + m_y \cdot m_y} \leq 10^{-12}$.

The extension for local hybrid functionals requires additional care, as the local mixing function (LMF) may depend on the kinetic energy density τ.[48,49,53] In this case, the LMF is constructed with the generalized kinetic energy density $\tilde{\tau}$ and the non-collinear approach [cf. Eqs. (8) and (9)].[53] The same applies for the two-component generalization[53] of the calibration function.[110,111] Note that the exact exchange contribution is evaluated semi-numerically on a grid.[100,112–114]

B. EPR properties with a common gauge origin

For EPR properties, such as the hyperfine coupling (HFC) tensor A and the g-tensor g with a common gauge origin, only the ground-state density matrix and the XC potential are required, i.e., no derivatives of the density matrix or the XC potential are needed,[115–120] and the tensors can be evaluated according to

$$A_{N,uv} = \left. \frac{\mathrm{d}^2E}{\mathrm{d}I_{N,u}\,\mathrm{d}S_v} \right|_{\vec{I}_N=0} = \frac{g_N\beta_N}{\tilde{S}_v} \left. \frac{\mathrm{d}E(J_v, \vec{m}_N)}{\mathrm{d}m_{N,u}} \right|_{\vec{m}_N=0}$$
$$= \frac{g_N\beta_N}{\tilde{S}_v} \mathrm{tr}\left[\mathbf{P}(J_v)\ \mathbf{h}^N_u \right], \tag{29}$$

$$g_{uv} = \left. \frac{\mathrm{d}^2E}{\mathrm{d}B_u\,\mathrm{d}S_v} \right|_{\vec{B}=0} = \frac{2c}{\tilde{S}_v} \left. \frac{\mathrm{d}E(J_v, \vec{B})}{\mathrm{d}B_u} \right|_{\vec{B}=0} = \frac{2c}{\tilde{S}_v} \mathrm{tr}[\mathbf{P}(J_v)\ \mathbf{h}^B_u], \tag{30}$$

where $\tilde{S}_v$ denotes the effective spin of the component v, J denotes the total angular momentum, g_N denotes the nuclear g-factor, β_N denotes Bohr's magneton, $\vec{I}_N$ denotes the spin of nucleus N, $\vec{m}_N$ denotes the respective nuclear magnetic moment, and $\vec{B}$ denotes the external magnetic field. The spin derivative is calculated with three independent SCF calculations using three orthogonal alignments of the spin. Essentially, the density matrix is contracted with the derivative of the one-electron Hamiltonian with respect to the nuclear magnetic moments or the external magnetic field. Additionally, the electric field gradient (EFG) and the nuclear quadrupole interaction tensor can be calculated as an expectation value with the proper picture-change correction.[120,121] Thus, a 2c SCF implementation of the CDFT ansatz is directly suitable for EPR spectroscopy.

A gauge-origin invariant implementation of the g-tensor necessitates GIAOs similar to NMR shieldings. Therefore, the derivative of the XC potential with respect to the magnetic field needs to be formed.[120,122] However, a gauge-origin invariant framework is only needed for systems with a spatially distributed spin excess density,[120,123] which is beyond the scope of the present work.

C. Exchange–correlation kernel for Kramers-restricted systems

The exchange–correlation kernel for Kramers-restricted systems can be formed similarly by using the chain rule in a

straightforward manner.[58] In this special case, $\mathbf{P}^{\alpha\alpha} = (\mathbf{P}^{\beta\beta})^\dagger$ holds. Therefore, only the (symmetric) real part of $\mathbf{M}^0$ and the (anti-symmetric) imaginary part of $\mathbf{M}^z$ need to be considered. These are exactly represented by the density matrix $\mathbf{P}^{\alpha\alpha}$. In the Kramers-restricted case, it is therefore advantageous to write the XC kernel equations in terms of the density matrix $\mathbf{P}$ instead of $\mathbf{M}$. Again, the LAOs reduce to real field-independent basis functions, and the kernel equation reads

$$\begin{aligned}\frac{\delta^2 E^{\mathrm{XC}}}{\delta P_{\mu\nu,k}\delta P_{\kappa\lambda,l}} = \iint \Bigg[&\frac{\partial^2 g^{\mathrm{XC}}}{\partial\rho_k\partial\rho_l}\frac{\partial\rho_k}{\partial P_{\mu\nu,k}}\frac{\partial\rho_l}{\partial P_{\kappa\lambda,l}} + \frac{\partial^2 g^{\mathrm{XC}}}{\partial\vec{\nabla}\rho_k\partial\vec{\nabla}\rho_l}\frac{\partial\vec{\nabla}\rho_k}{\partial P_{\mu\nu,k}}\frac{\partial\vec{\nabla}\rho_l}{\partial P_{\kappa\lambda,l}} + \frac{\partial^2 g^{\mathrm{XC}}}{\partial\tilde{\tau}_k\partial\tilde{\tau}_l}\frac{\partial\tilde{\tau}_k}{\partial P_{\mu\nu,k}}\frac{\partial\tilde{\tau}_l}{\partial P_{\kappa\lambda,l}} + \frac{\partial^2 g^{\mathrm{XC}}}{\partial\rho_k\partial\vec{\nabla}\rho_l}\frac{\partial\rho_k}{\partial P_{\mu\nu,k}}\frac{\partial\vec{\nabla}\rho_l}{\partial P_{\kappa\lambda,l}} \\ &+ \frac{\partial^2 g^{\mathrm{XC}}}{\partial\vec{\nabla}\rho_k\partial\rho_l}\frac{\partial\vec{\nabla}\rho_k}{\partial P_{\mu\nu,k}}\frac{\partial\rho_l}{\partial P_{\kappa\lambda,l}} + \frac{\partial^2 g^{\mathrm{XC}}}{\partial\rho_k\partial\tilde{\tau}_l}\frac{\partial\rho_k}{\partial P_{\mu\nu,k}}\frac{\partial\tilde{\tau}_l}{\partial P_{\kappa\lambda,l}} + \frac{\partial^2 g^{\mathrm{XC}}}{\partial\tilde{\tau}_k\partial\rho_l}\frac{\partial\tilde{\tau}_k}{\partial P_{\mu\nu,k}}\frac{\partial\rho_l}{\partial P_{\kappa\lambda,l}} + \frac{\partial^2 g^{\mathrm{XC}}}{\partial\vec{\nabla}\rho_k\partial\tilde{\tau}_l}\frac{\partial\vec{\nabla}\rho_k}{\partial P_{\mu\nu,k}}\frac{\partial\tilde{\tau}_l}{\partial P_{\kappa\lambda,l}} \\ &+ \frac{\partial^2 g^{\mathrm{XC}}}{\partial\tilde{\tau}_k\partial\vec{\nabla}\rho_l}\frac{\partial\tilde{\tau}_k}{\partial P_{\mu\nu,k}}\frac{\partial\vec{\nabla}\rho_l}{\partial P_{\kappa\lambda,l}} + \frac{\partial g^{\mathrm{XC}}}{\partial\tilde{\tau}_k}\frac{\partial^2\tilde{\tau}_k}{\partial\rho_k\partial\vec{j}_{\mathrm{p},k}}\left(\frac{\partial\rho_k}{\partial P_{\mu\nu,k}}\frac{\partial\vec{j}_{\mathrm{p},k}}{\partial P_{\kappa\lambda,k}} + \frac{\partial\vec{j}_{\mathrm{p},k}}{\partial P_{\mu\nu,k}}\frac{\partial\rho_k}{\partial P_{\kappa\lambda,k}}\right) + \frac{\partial g^{\mathrm{XC}}}{\partial\tilde{\tau}_k}\frac{\partial^2\tilde{\tau}_k}{\partial\rho_k^2}\frac{\partial\rho_k}{\partial P_{\mu\nu,k}}\frac{\partial\rho_k}{\partial P_{\kappa\lambda,k}} \\ &+ \frac{\partial g^{\mathrm{XC}}}{\partial\tilde{\tau}_k}\frac{\partial^2\tilde{\tau}_k}{\partial(\vec{j}_{\mathrm{p},k})^2}\frac{\partial\vec{j}_{\mathrm{p},k}}{\partial P_{\mu\nu,k}}\frac{\partial\vec{j}_{\mathrm{p},k}}{\partial P_{\kappa\lambda,k}}\Bigg]\mathrm{d}^3r\ \mathrm{d}^3r'. \end{aligned} \tag{31}$$

Here, k and l mark that the derivative could be taken with respect to two different density matrices, but usually they coincide up to the corresponding spinor cases. A detailed discussion and recipe for the implementation of Eq. (31) is provided in Ref. 58. We note that excited states can carry currents even if the ground-state current density vanishes, which was already considered by Bates and Furche.[95] However, the CDFT framework leads to additional terms, which were previously neglected.[28,113,124] For instance, Eq. (31) gives rise to coupling terms of two currents, yielding quadratic and $\vec{j}_{\mathrm{p}}^{\,4}$ dependent terms.[58]

The local hybrid exchange–correlation kernel is extended similarly. Currently, we neglect the calibration function in the two-component kernel.[28] So far, this is only relevant for LH14t-calPBE,[110] LH20t,[52] and LHJ-HFcal.[53] The other implemented functionals, such as LH07t-SVWN,[125] LH07s-SVWN,[126] LH12ct-SsirPW92,[127] LH12ct-SsifPW92,[127] LH20t*,[52] mPSTS-a1,[51,100] mPSTS-noa2,[51,100] Johnson's 2014 local hybrid (LHJ14),[50] LHJ-HF,[53] Tao-Mo-Holzer-Franzke (TMHF),[53] and TMHF-3P[53] as well as the parent local hybrids Lh-BLYP and Lh-PBEPKZB,[48] do not make use of a calibration function.

D. Implementation

The current density functional framework for spin–orbit coupling was implemented in the TURBOMOLE quantum chemistry program suite.[47,128–130] The implementation is based on the machinery developed for strong magnetic fields[58,131–133] as well as the existing 2c *meta*-GGA[26,124] and LHF routines[28,53,100,112,113] with the standard kinetic energy density. Interfaces for Libxc[134–136] and XCFun[137] are available to allow for calculations with (almost) all presented density functional approximations. Shared-memory parallelization is supported by the OpenMP standard throughout the SCF procedure and all properties.[138,139]

Note that the generalized kinetic density and the paramagnetic current density require reworked thresholds. We have tightened the internal thresholds for the screening procedure[109,140] by three orders of magnitude, as previously done for local hybrids in Ref. 101. This avoids oscillating energies during the SCF procedure.

Herein, we have implemented the spin–orbit coupling CDFT approach for ground-state energies and densities, which also allows us to calculate EPR properties.[119,120] Additionally, geometry gradients are implemented for *meta*-GGAs by extension of the existing machinery.[26,141] Furthermore, CDFT is available for the XC kernel of excitation energies from time-dependent density functional theory (TD-DFT)[124] and the correlation kernel augmented Bethe–Salpeter equation (cBSE),[142] NMR spin–spin coupling constants,[101,102] as well as static, dynamic, and damped polarizabilities.[28] Additionally, the XC kernel is the only relevant DFT ingredient for NMR shieldings and shifts with a common gauge origin.[143] A respective X2C implementation is briefly discussed in the supplementary material.

III. COMPUTATIONAL DETAILS

First, we apply the CDFT approach for spin–orbit coupling to the ground-state energies of metal clusters. The impact of the current density on the stability of small bismuth cluster cations of up to 14 atoms is considered.[144] The structures are taken from the Ref. 144, and all calculations are carried out as described therein. Dirac–Fock effective core potentials are used to model the inner 60 electrons of each bismuth atom (ECP60MDF).[145] This is combined with a two-component self-consistent procedure to account for spin–orbit coupling. All calculations are performed on the Tao-Perdew-Staroverov-Scuseria (TPSS)/dhf-TZVP-2c level of theory.[146,147] Fine grids (grid 5) are employed for the numerical integration.[109,140] The resolution of the identity approximation[19,148–150] (RI-J) is used with tailored auxiliary bases,[151] and the SCF procedures are converged up to at least 10^{-8} E_{h}. Additionally, we employ the TASK density functional[152] using Libxc.[134–136]

Second, the excitation energies of the molecules I_2, TlH, AuH, HfO, $[PdCl_4]^{2-}$, $[PtCl_4]^{2-}$, $[Re(bpy)(CO)_3I]$ (bpy = 2,2′-bipyridine), UO_2^{2+}, $[UO_2Cl_4]^{2-}$,[153] and $[W_6O_{19}]^{2-}$[154] are calculated. The local exact two-component (DLU-X2C) Hamiltonian is employed with the finite nucleus model and the modified screened nuclear spin–orbit (mSNSO) correction.[28,141,155] We use the x2c-TZVPall-2c orbital[156] and auxiliary basis sets for all atoms but

uranium.[156,157] For uranium, the cc-pVQZ-X2C basis set is used.[158] For excited states, the semi-numerical semiJK algorithm is used to calculate Coulomb and exact exchange parts.[113] We employ the Tao-Mo,[159] TASK,[152] TPSS,[146] TPSSh,[146,160] r^{2}SCAN,[161,162] r^{2}SCAN0,[161–163] B97M,[164] ωB97M,[165] M06-L,[166] M06,[167] and M06-2X[167] meta-GGA density functional approximations with large grids (grid 4a).[109,140,168] LH12ct-SsirPW92 (denoted LH12ct),[127] LHJ14,[50] and TMHF[53] serve as examples for local hybrid functionals. Throughout this work, Libxc[134–136] is used for all *meta*-GGA functionals except TPSS and TPSSh. SCF procedures are converged to at least 10^{-9} E_h for the energy and 10^{-8} a.u. for the root mean square of the norm of the density matrix. A threshold of 10^{-6} a.u. for the norm of the residuum indicates convergence in the coupled-perturbed Kohn–Sham (CPKS) equations.

Third, the isotropic NMR shielding and (reduced) spin–spin coupling constants of the hydrogen halides HX (X = F, Cl, Br, I, and At) are calculated. The first are obtained with the X2C Hamiltonian in a restricted magnetically balanced basis set[143] with a common gauge origin at the heavy atom. For the NMR couplings,[101,102] we use the restricted kinetic balance condition.[169] The finite nucleus model for both the scalar and the vector potential and the modified screened nuclear spin–orbit approximation[170–173] are used throughout. Parameters for the Gaussian charge distribution are taken from Ref. 174. We use the x2c-QZVPall-2c-s orbital[157] and auxiliary basis sets[156,157] for the resolution of the identity approximation (RI-*J*). SCF procedures are converged to at least 10^{-8} E_h, and a threshold of 10^{-7} a.u. indicates convergence in the CPKS equations. The same functionals and grids as for the TD-DFT study are applied. Structures are taken from Refs. 175 and 176. Further studies on the NMR coupling constants of TtH_4 (Tt = C, Si, Ge, Sn, and Pb) are presented in the supplementary material. Therein, we also show results for the ^{31}P NMR properties of the low-valent Sn compound [({SIDipp}P)$_2$Sn] [with SIDipp = 1,3-bis(2,6-diisopropylphenyl)-imidazolidin-2-ylidene] of Ref. 177.

Fourth, the EPR hyperfine coupling constant and isotropic Δg-shift of the transition-metal complexes $[MoNCl_4]^{2-}$, $[MoOF_4]^-$, $[MoOCl_4]^-$, $[MoOF_5]^{2-}$, $[MoOBr_5]^{2-}$, $[WOCl_4]^-$, $[WOF_5]^{2-}$, $[WOBr_5]^{2-}$, $[TcNF_4]^-$, $[TcNCl_4]^-$, $[TcNBr_4]^-$, $[ReNF_4]^-$, $[ReNCl_4]^-$, $[ReNBr_4]^-$, $[ReOBr_4]$, $[ReOF_5]^-$, and $[OsOF_5]$ are calculated. We use the same settings as in Refs. 53, 119, and 120. Therefore, the X2C Hamiltonian in the diagonal local approximation to the unitary decoupling transformation (DLU) is employed,[97,101,119,120,141,155,178,179] which allows for large-scale applications[180,181] with substantially reduced computational costs. We use the finite nucleus model for the scalar potential and the vector potential[174] and the mSNSO approximation.[170–173] All compounds feature one metal center. Consequently, a common gauge origin placed at the metal center is sufficient, and we use the restricted magnetic balance condition[143] for the g-tensor. The x2c-QZVPall-2c basis set is used for all elements,[157] and the conductor-like screening model (COSMO) is applied with the default parameters to compensate the negative charge.[182,183] Very large grids (grid 5a) are employed.[109,140,168] Structures are taken from Ref. 117, and SCF energies are converged with a threshold of 10^{-9} E_h. We consider the same *meta*-GGA-based functionals as for the TD-DFT and NMR study. Additionally, we use three local hybrid functionals, namely, LHJ14,[50] LH20t,[52] and TMHF.[53] Results with the standard kinetic energy density and the TPSS,[146] TPSSh,[146,160] r^{2}SCAN,[161,162] r^{2}SCAN0,[161–163] LHJ14,[50] LH20t,[52] and TMHF[53] functionals are taken from Refs. 53, 119, and 120. The nuclear g-factors are −0.365 389 0 (^{95}Mo), 0.235 569 6 (^{183}W), 1.263 201 9 (^{43}Tc), 1.287 881 3 (^{187}Re), and 0.439 955 5 (^{189}Os).

Fifth, the hyperfine coupling constant of $[TbPc_2]^-$, Pc = bis(phthalocyaninato) and g_N = 1.342 752 3 for ^{159}Tb, with six unpaired electrons is studied. Here, the paramagnetic spin–orbit term is the leading contribution.[119,184] The structure is taken from Refs. 184 and 185. Calculations are performed with the Tao-Mo,[159] TPSS,[146] TPSSh,[146,160] r^{2}SCAN,[161,162] r^{2}SCAN0,[161–163] B97M,[164] ωB97M,[165] LHJ14,[50] and TMHF[53] functionals. LH20t[52] is excluded as the calibration function leads to an unfavorable 2c SCF behavior, and the SCF procedure did not converge in 300 cycles and 12 days on 24 OpenMP threads of an Intel® Xeon® Gold 6212U central processing unit (CPU) @ 2.40 GHz. We use similar but tighter computational settings than in Ref. 119. The mSNSO-DLU-X2C Hamiltonian[97,101,119,141,155,178,179] in the finite nucleus model[174] is applied together with the x2c-TZVPPall-2c basis set for Tb[156] and the x2c-SVPall-2c basis set for the other elements.[156] This basis set was shown to be sufficient for the Tb HFC constant.[119] Very large grids (grid 5a) are employed.[109,140,168] Moreover, the reduction of spherical grid points near a nucleus (pruning) is suppressed. The SCF procedure is converged with thresholds of 10^{-7} E_h for the energy and 10^{-7} a.u. for the root mean square of the density matrix. COSMO is applied with the settings for tetrahydrofurane (THF), i.e., a permittivity of ε_r = 7.520, a refraction index of n = 1.4050, a solvation radius of 1.30 Å, and the default radii for the atoms.[182,183] Additional calculations of La(II) and Lu(II)-based single molecule magnets[186] are presented in the supplementary material. There, we discuss the HFC tensor, the g-tensor, as well as the electric field gradient and the nuclear quadrupole interaction tensor.

IV. RESULTS AND DISCUSSION

A. Ground-state energies of bismuth cluster cations

In order to assess the impact of the ground-state current density on molecular properties, we first investigate how ground-state energies and properties are impacted. In Ref. 144, Kelting *et al.* presented experimental studies and quantum chemical calculations on small bismuth cluster cations. For these calculations, a two-component approach was used in order to capture the effects induced by spin–orbit coupling. The aim of this investigation was to analyze the relative stability of different isomers, ΔE_{stab}. The *meta*-GGA functional TPSS was used without considering the ground-state current density, i.e., $E_{SO}[\vec{j}_p = 0]$. In this section, we revisit the investigation of bismuth cluster cations from Ref. 144, additionally taking the self-consistent relaxation of the ground-state current density into account as previously described in Sec. II A. We, thus, compare the total energy including spin–orbit coupling with a relaxed current density, $E_{SO}[\vec{j}_p]$, to the treatment without considering $\vec{j}_p$. The difference between these two quantities (that is, the impact of the current density on the total energy) is presented in Table I as ΔE_{CDFT}. Moreover, the relative stability of isomers is calculated both without considering the current density, $\Delta E_{stab}[\vec{j}_p = 0]$, and with its relaxed counterpart, $\Delta E_{stab}[\vec{j}_p]$.

TABLE I. Relative energies for different isomeric structures of small bismuth cluster cations in meV with the TPSS and TASK density functional approximations. The change in energy due to the consideration of the ground-state current density is listed for all systems as ΔE_{CDFT}. CDFT always leads to lower SCF energy, i.e., the energy becomes more negative. The relative stability of isomers with respect to the energetically most favored isomer is shown both without taken the current density into account, $\Delta E_{stab}[\vec{j}_p = 0]$, and with its explicit consideration, $\Delta E_{stab}[\vec{j}_p]$. All structures are taken from Ref. 144. Point group symmetry is not exploited in two-component calculations. All values are in meV.

			TPSS			TASK		
Cluster	Isomer	Point group	ΔE_{CDFT}	$\Delta E_{stab}[\vec{j}_p = 0]$	$\Delta E_{stab}[\vec{j}_p]$	ΔE_{CDFT}	$\Delta E_{stab}[\vec{j}_p = 0]$	$\Delta E_{stab}[\vec{j}_p]$
Bi_4^+	I	D_{2d}	18.0	⋯	⋯	173.8	⋯	⋯
Bi_5^+	I	C_{4v}	19.7	⋯	⋯	186.6	⋯	⋯
	II	D_{3h}	32.1	508.4	496.0	352.4	724.5	558.7
Bi_6^+	I	C_2	29.0	⋯	⋯	284.5	⋯	⋯
	II	C_s	29.3	24.8	24.5	283.1	−118.0	−116.5
	III	C_{2v}	24.7	31.7	36.0	241.0	−204.7	−161.2
	IV	C_2	31.8	91.7	88.9	314.5	−225.2	−255.3
Bi_7^+	I	C_s	30.6	⋯	⋯	296.0	⋯	⋯
	II	C_{3v}	29.8	532.3	533.1	286.4	668.6	678.2
Bi_8^+	I	D_{4d}	42.7	⋯	⋯	414.5	⋯	⋯
	II	C_s	36.4	139.9	146.2	348.5	−548.3	−482.3
Bi_9^+	I	C_{3v}	39.3	⋯	⋯	379.5	⋯	⋯
	II	C_s	37.9	172.4	173.7	360.1	512.9	532.3
	III	C_{3h}	39.8	225.6	225.0	388.6	618.7	609.6
	IV	C_S	39.2	259.7	259.7	384.3	185.8	181.0
Bi_{10}^+	I	C_{2v}	53.2	⋯	⋯	505.4	⋯	⋯
	II	C_s	47.1	159.5	165.5	452.0	−675.0	−621.5
Bi_{11}^+	I	C_2	47.4	⋯	⋯	453.4	⋯	⋯
	II	C_s	47.8	117.3	116.8	463.9	−405.3	−415.8
Bi_{12}^+	I	C_s	56.7	⋯	⋯	538.8	⋯	⋯
	II	C_s	53.7	33.9	36.8	519.8	138.6	157.6
Bi_{13}^+	I	C_s	58.6	⋯	⋯	566.2	⋯	⋯
	II	C_1	57.9	34.9	35.6	559.0	−132.1	−124.9
	III	C_1	57.5	77.4	78.5	552.4	−277.8	−264.0
	IV	C_1	56.8	64.4	66.2	545.5	42.7	63.5
Bi_{14}^+	I	C_1	64.1	⋯	⋯	603.9	⋯	⋯
	II	C_s	61.2	−2.4	0.5	572.1	−262.0	−230.2
	III	C_s	64.5	242.7	242.3	615.9	344.8	332.8

Evidently, the relaxation of the ground-state current does have an impact on the total electronic energy, regardless of whether the systems exhibit Kramers symmetry. In a Kramers-restricted framework, the real and symmetric matrices in Eqs. (12)–(14) are zero. However, their anti-symmetric counterparts used for the current density are not and CDFT consequently leads to energy changes for closed-shell systems. The energy associated with a ground-state current relaxation is of the order of a few dozen meV for these clusters, increasing in magnitude with an increasing cluster size. Following the variation principle, the inclusion and relaxation of the current density always results in a lower energy. The relative stability of isomers, however, is less affected by the relaxation of the ground-state current due to error compensation. For Bi_5^+, the deviation is ∼12 meV, which amounts to an overall deviation of more than 2%. The interplay between the structure and the impact of the current density is illustrated by the relative energies of the isomers of Bi_6^+. Here, isomer II is only slightly affected as the relative stabilization of isomer I decreases from 24.8 to 24.5 meV. However, a large change is observed for isomer III with a rise from 31.7 to 36.0 meV. That constitutes an increase by almost 14%. The two isomers of Bi_8^+ are also particularly affected, exhibiting a deviation of about 6 meV for the relative stability, which amounts to more than 4%. Other systems, such as the four isomers of Bi_9^+, show significantly less impact of a ground-state current relaxation, with deviations well below 1%.

The impact of the current density drastically depends on the density functional approximation. TPSS shows a modest dependence on the current density for magnetic properties.[98] Therefore, we repeat the same calculations with the TASK functional. These results are listed in Table I as well. Significantly larger discrepancies between $\Delta E_{stab}[\vec{j}_p = 0]$ and $\Delta E_{stab}[\vec{j}_p]$ can be observed. The stability of isomer I of Bi_5^+ is severely overestimated if the ground-state current is neglected, with a deviation of 166 meV (around 30%). A similarly large deviation occurs for the relative stability of isomer III of Bi_6^+, where the stability of the isomer is overestimated by 43.5 meV (about 27%). Other cases are less problematic, but

deviations of up to 30% are not uncommon for the relative stabilities of the respective isomers. We also note that TASK changes the energetic order of the isomers for Bi_6^+, Bi_8^+, Bi_{10}^+, Bi_{11}^+, Bi_{13}^+, and Bi_{14}^+. The largest changes between TPSS and TASK are observed for Bi_{10}^+. Isomer I (C_{2v}) is more stable than isomer II (C_s) by about 160 meV with TPSS. However, the latter isomer is lower in energy by more than 600 meV with TASK. This shows a substantial dependence of the cluster cations on the density functional approximation.

To summarize, the impact of the ground-state current density on the total energy is small. Yet, the error by not considering the current is clearly not negligible for all isomers. This particularly affects relative energies and stabilities, which are target quantities in many fields of quantum chemistry. Moreover, Kramers-symmetric closed-shell systems suffer from the same errors as open-shell systems. In general, it is advisable to consider the self-consistent relaxation of the ground-state current density for systems with pronounced spin–orbit coupling.

B. Excitation energies from TD-DFT

For excitation energies, the influence of the current density on valence excitations is generally negligible. The mean average deviations and maximum deviations found for eight of the ten investigated molecules, all of them involving metal centers, are well below 0.05 eV. Compared to the general error of TD-DFT, which is up to 0.3 eV even for good density functionals, the additional kernel terms are not too important. This is in line with the findings of Bates and Furche[95] and also with the more recent study of Liang *et al.*[96] Contrarily, it was already suspected that relativistic effects may amplify the impact of the current density.[58,95] This can be confirmed especially for non-hybrid *meta*-GGA functionals, as shown in Table II.

Table II shows that especially functionals that strongly depend on the kinetic energy density τ are largely impacted by adding the current-dependent terms. As previously observed for paramagnetic NMR properties,[102] the results for TASK are most strongly altered, followed by M06-L and r^{2}SCAN. The mean and median deviations range up to 0.15 and 0.14 eV, outlining that the changes are quite significant even compared to the usual error bars of TD-DFT, set to 0.3–0.4 eV. The high median deviations also suggest that the influence is not caused by a few outliers, but rather systematic. By investigating the differences for every system individually, it also becomes clear that the shift for a functional is not uniform.

Figure 1 outlines the deviations caused by neglecting the paramagnetic current density for the TASK functional. Clearly, some molecules are more affected than others. The largest deviation is found for TlH, where it can reach nearly 0.8 eV. In-between are AuH, the palladium and platinum chloride anions, as well as the uranyl complexes, where deviations of roughly 0.3 eV are found. In contrast, the rhenium complex [Re(bpy)(CO)$_3$I] is hardly affected at all, and also for the tungsten oxide anion, only minor effects are observed. This is a rather critical result: TASK aims at describing non-locality and related effects and does so by enforcing large variants of the enhancement factor F_X with respect to the kinetic energy density τ. Therefore, semi-local functionals that aim at recovering charge-transfer (CT) excitations will be heavily affected by the current-dependent modification of the kinetic energy density, even for non-CT excited states. For these functionals, an appropriate modification of τ, therefore, must be considered.

For hybrid functionals, the impact of $\vec{j}_p$ is quickly reduced. For example, TPSSh has roughly only half the variation of TPSS. Some hybrids, such as TPSSh, may on average not see a lot of changes, but still spikes in deviation are obtained. These spikes range from 0.05 to 0.1 eV, making them less pronounced than the errors of semi-local functionals, yet still significant. Additionally, the general sign of the deviation is flipped for some hybrid functionals and molecules, yielding blue-shifts upon incorporating the current density. For semi-local functionals, only red-shifts are observed.

TABLE II. Impact of the current-dependent generalization of τ on the excitation energies of molecular systems. Given are the mean absolute deviation (MAD), standard deviation (STD), and maximum absolute deviation (Max). All values are in eV.

	MAD	STD	Max.
Tao-Mo	0.015	0.025	0.199
TPSS	0.014	0.018	0.091
TPSSh	0.013	0.016	0.048
r^{2}SCAN	0.055	0.075	0.314
r^{2}SCAN0	0.044	0.057	0.208
B97M	0.050	0.045	0.199
ωB97M	0.022	0.032	0.119
TASK	0.147	0.212	0.810
M06-L	0.031	0.046	0.160
M06	0.041	0.071	0.303
M06-2X	0.044	0.053	0.189
LH12ct	0.017	0.034	0.186
LHJ14	0.029	0.039	0.127
TMHF	0.006	0.009	0.065

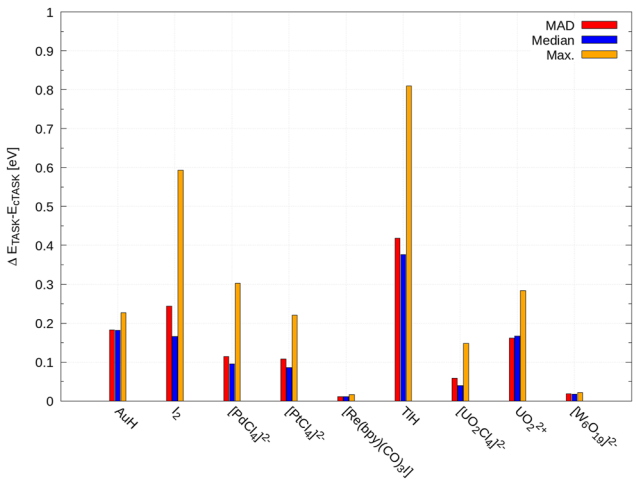

FIG. 1. Mean absolute deviation (MAD) and median deviation and maximum deviation (Max.) for the investigated molecules at the TASK/x2c-TZVPPall-2c level of theory with and without the paramagnetic current density $\vec{j}_p$. Note that HfO is not shown, as it becomes unstable without $\vec{j}_p$. All values are in eV.

TABLE III. Impact of the current-dependent generalization of τ on the isotropic NMR shielding constants and reduced NMR coupling constants. The atom label denotes the NMR shielding constant and K refers to the reduced spin–spin coupling constant in 10^{19} T^2/J. Experimental findings are taken from Refs. 187–190 as collected in Ref. 191. See this reference for details on absolute NMR shieldings. We have excluded σ(I) for HI, as this value is obtained from a combination of an experimental spin-rotation constant and the calculated diamagnetic shielding constant. This is not easily applicable to heavy elements.[76,191] Note that the result for K(H–F) of Ref. 187 is extrapolated to the equilibrium distance.

	HF			HCl			HBr			HI			HAt		
	σ(F)	σ(H)	K(H–F)	σ(Cl)	σ(H)	K(H–Cl)	σ(Br)	σ(H)	K(H–Br)	σ(I)	σ(H)	K(H–I)	σ(At)	σ(H)	K(H–At)
Tao-Mo	413.40	29.69	29.30	978.72	31.81	19.62	2925.78	36.18	−35.23	5848.30	45.33	−99.03	17 346.17	64.26	−614.30
cTao-Mo	413.05	29.99	29.41	977.61	32.18	19.69	2923.90	36.53	−35.05	5845.75	45.70	−98.63	17 349.25	64.94	−613.83
TPSS	413.27	29.60	33.97	971.43	31.78	20.11	2899.11	36.24	−32.22	5787.54	45.36	−88.73	17 204.20	64.50	−540.90
cTPSS	412.48	29.88	34.14	969.92	32.22	20.18	2897.29	36.69	−32.07	5786.06	45.87	−88.37	17 205.63	65.17	−539.84
TPSSh	414.22	29.41	35.81	974.19	31.66	20.84	2910.07	36.08	−29.87	5810.85	45.29	−88.09	17 342.69	65.02	−586.50
cTPSSh	413.51	29.65	35.96	972.85	32.05	20.90	2908.46	36.48	−29.74	5809.53	45.75	−87.77	17 344.33	65.64	−585.58
r^{2}SCAN	419.18	28.88	29.14	994.79	31.04	20.52	2956.63	35.21	−28.88	5913.21	44.66	−117.79	17 561.86	65.23	−804.08
cr^{2}SCAN	416.00	29.39	30.10	989.22	31.63	21.03	2946.94	35.86	−28.02	5898.57	45.50	−116.35	17 545.91	67.14	−802.09
r^{2}SCAN0	419.63	28.63	35.47	993.38	31.05	22.47	2962.59	35.27	−23.71	5928.31	45.09	−110.89	17 799.68	67.00	−881.69
cr^{2}SCAN0	417.41	28.96	36.15	989.74	31.42	22.80	2956.19	35.68	−23.13	5918.59	45.63	−109.91	17 790.63	68.32	−880.73
B97M	419.39	28.66	37.80	994.39	30.91	19.95	2944.24	35.14	−50.92	5857.69	44.81	−133.09	17 575.83	63.21	−694.61
cB97M	414.97	29.38	38.91	985.79	31.59	20.59	2930.91	35.79	−49.92	5841.05	45.53	−131.57	17 565.09	64.55	−691.76
ωB97M	416.54	29.36	34.05	977.14	32.02	20.97	2916.92	36.21	−18.09	5826.39	45.57	−82.56	17 612.40	65.81	−653.55
cωB97M	415.70	29.36	34.24	976.87	31.81	20.99	2916.55	35.97	−18.09	5826.10	45.23	−82.67	17 602.26	65.23	−652.88
TASK	424.45	28.31	22.23	1011.43	30.28	32.34	2977.01	33.87	−9.47	5902.08	42.45	−94.30	17 340.25	62.59	−722.85
cTASK	418.15	29.14	24.13	1001.43	31.37	33.29	2955.99	35.17	−7.77	5867.40	44.25	−91.35	17 298.47	66.54	−718.12
M06-L	419.57	28.90	48.98	995.25	31.02	32.22	2923.91	35.11	−15.32	5798.67	42.47	8.51	17 204.20	64.50	−540.90
cM06-L	416.06	29.47	49.85	989.35	31.69	32.64	2915.06	35.89	−14.75	5789.02	43.43	9.36	17 205.63	65.17	−539.84
M06	415.24	29.16	54.63	967.74	32.03	38.66	2884.17	36.16	−39.81	5749.25	44.21	−70.40	17 552.73	61.72	−421.19
cM06	414.85	29.10	54.66	968.97	31.92	38.54	2887.24	36.10	−40.09	5759.82	44.08	−71.04	17 564.43	60.83	−421.98
M06-2X	412.54	29.54	38.08	966.02	32.36	30.53	2916.95	36.39	66.38	5816.44	46.41	36.30	17 599.13	71.58	−976.53
cM06-2X	415.76	29.12	37.19	972.77	31.79	30.05	2924.21	35.85	65.79	5821.07	45.80	35.54	17 581.89	70.64	−975.69
LH12ct	423.04	28.51	36.29	996.07	31.02	17.10	2960.69	34.55	−17.46	5894.12	42.64	−71.64	17 609.83	61.30	−554.21
cLH12ct	422.61	28.60	36.45	995.35	30.96	17.23	2957.40	34.45	−17.20	5887.45	42.53	−71.29	17 601.15	61.49	−554.90
LHJ14	414.93	29.53	38.10	965.93	32.19	18.49	2884.46	36.77	−28.77	5761.64	46.70	−89.22	17 357.78	67.89	−589.99
cLHJ14	416.02	29.36	37.78	968.72	31.91	18.29	2889.31	36.45	−29.13	5769.79	46.26	−89.87	17 364.89	66.98	−590.53
TMHF	417.43	29.20	44.40	979.78	32.08	24.77	2926.37	36.71	−32.75	5847.68	46.72	−99.64	17 728.88	68.67	−742.67
cTMHF	417.89	29.10	44.26	980.53	31.73	24.74	2924.90	36.39	−32.72	5843.96	46.39	−99.66	17 718.99	68.39	−742.59
Expt.	410	28.51	44.2	952	31.06	⋯	2617	34.96	⋯	⋯	43.86	⋯	⋯	⋯	⋯

Another notable effect can be observed for many of the investigated semi-local functionals. The current density becomes strikingly important for HfO, as the ground state is deemed unstable if the current is neglected. Furthermore, r^{2}SCAN also shows an instability for UO_2^{2+} if the paramagnetic current density is neglected. Given this severe uncertainty of a possible identification of an unstable ground state, even though it is actually stable, current density terms need to be included in 2c *meta*-GGA and local-hybrid-based TD-DFT calculations.

C. NMR properties of hydrogen halides

Results for the isotropic NMR shielding constants and reduced spin–spin coupling constants are listed in Table III. The impact of the current density on the coupling constant is almost negligible. Notable exceptions are again observed for TASK. For instance, the ^{1}K(H–F) coupling changes by 2×10^{19} T^2/J, equaling almost 10%. This confirms the observations in Sec. IV B. The comparably pronounced dependence of the current density on TASK also holds for the shielding constants of HF. For hydrogen, the shielding constant changes by almost 1 ppm from 28.31 to 29.14 ppm. For all other functionals, the changes are typically in the range of 1%–3%. This is in line with the previous finding that the current density generalization from τ to $\tilde{\tau}$ is more important for open-shell systems than for closed-shell systems.[98] For open-shell molecules, the current density induced by spin–orbit in the ground state is considerable, and therefore, the coupling of the current in this state with the excited states is also more pronounced. For closed-shell systems, the main contribution stems from the terms with $\vec{j}_p$ in the excited states of the XC kernel.

D. EPR properties of small transition-metal complexes

The mean absolute percent-wise deviation (MAPD) for the isotropic hyperfine coupling constant and Δg shift with respect to the experimental findings[192–203] of the transition-metal complexes are shown in Figs. 2 and 3. For the HFC, the current density functional framework leads to no real improvement, and the results are almost unaffected by the additional terms in the exchange–correlation potential. This is due to the comparably small contribution of the paramagnetic spin–orbit (PSO) contribution[97,117,119] for these complexes. The scalar-relativistic Fermi-contact contribution is by far the dominating term. Thus, spin–orbit interactions and current-dependent terms are of minor importance for many of these complexes.

Matters are different for the g-tensor, as this quantity is defined via spin–orbit coupling, i.e., all non-trivial terms of the g-tensor essentially arise due to spin–orbit perturbations.[97,204–206] Here, the current density leads to notable changes in the MAPD of 6.5% and 5.2% for r^{2}SCAN and r^{2}SCAN0, respectively. B97M shows the largest change by a reduction of the MAPD from 34.43% to 25.17%. For TPSS, TPSSh, and Tao-Mo, much smaller changes of 1.0%–2.7% are observed. Still, the current density improves the results in all of these cases.

At first glance, only the standard deviation of TASK is affected by the current density. The sharp increase can be mainly attributed to $[MoOBr_5]^{2-}$. The MAPD with respect to the experiment does not change notably, which is in stark contrast with the previous results presented herein and in our previous work using a perturbative ansatz.[98] The largest changes of the individual results is again found for TASK. However, the impact of the current density on the MAPD with respect to the experiment cancels out. CDFT substantially improves the results for the 4d complexes, whereas it leads to a serious deterioration for the 5d complexes. Therefore, the impact of the CDFT framework with respect to the parent density functional is shown in Fig. 4. TASK, M06-L, B97M, M06-2X, r^{2}SCAN, and r^{2}SCAN0 are substantially affected by the current density, while almost no change is found for TPSS, TPSSh, M06, ωB97M, and the Tao-Mo functional. These findings are in line with our previous observations, with the sensitivity closely resembling the dependence

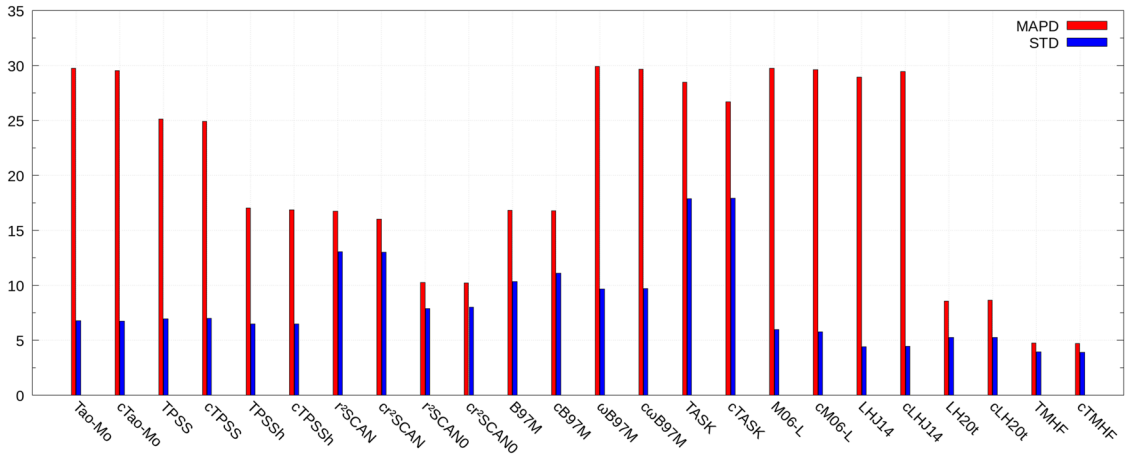

FIG. 2. Assessment of various (current) density functional approximations for the HFC constant compared to the experimental findings for a set of 12 transition-metal complexes.[117] MAPD and STD denote the mean absolute percent-wise error and its standard deviation. The data of the conventional functionals are partly taken from Ref. 119. See the supplementary material for results with the Minnesota hybrid functionals M06 and M06-2X.

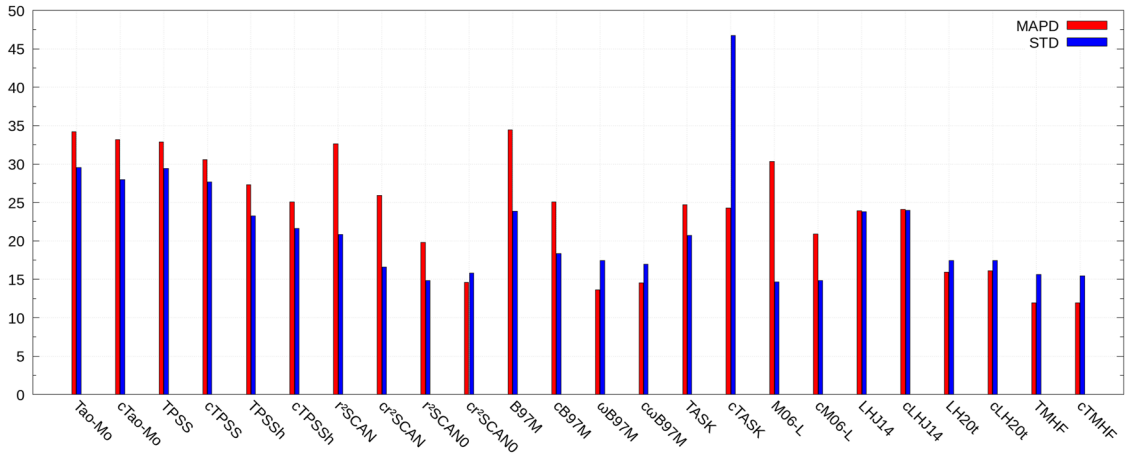

FIG. 3. Assessment of various (current) density functional approximations for the Δg-shift compared to the experimental findings for a set of 17 transition-metal complexes.[117] MAPD and STD denote the mean absolute percent-wise error and its standard deviation. The data of the conventional functionals are partly taken from Ref. 120. See the supplementary material for results with the Minnesota hybrid functionals M06 and M06-2X. Shifts below 5 ppt are neglected in the statistical evaluation.

of the current density on the enhancement factor.[98] Incorporating exact exchange again weakens the dependence on the current density. This is stressed by the results of the local hybrid functionals LHJ14, LH20t, and TMHF. The results outline that the current-dependent ansatz is mainly of formal importance for local hybrid functionals, as it ensures the iso-orbital constraint with magnetic perturbations.[95]

E. Hyperfine coupling constant of $[TbPc_2]^-$

Increasing the number of unpaired electrons generally leads to an increasing contribution from the PSO term. Thus, the impact of spin–orbit coupling and the current density is also expected to increase. Table IV lists the isotropic hyperfine coupling constant of $[TbPc_2]^-$, depicted in Fig. 5 with six unpaired electrons. Perturbative treatment of spin–orbit coupling clearly breaks down and leads to large deviations from the self-consistent two-component treatment. This effect is more pronounced for the current-dependent version of the tested functionals, leading to an iterative procedure for the solution of the response equations with semi-local functionals. Without the current density response, no iterations are required due to symmetry reasons.[97] In line with the expectations, larger changes are evident for the current density functionals. For TPSS and TPSSh, the HFC constant changes by about 10% or 30 MHz in the 2c CDFT framework, whereas a change of 60 MHz is observed for r^2SCAN. The B97M family represents an intermediate case. The finding that

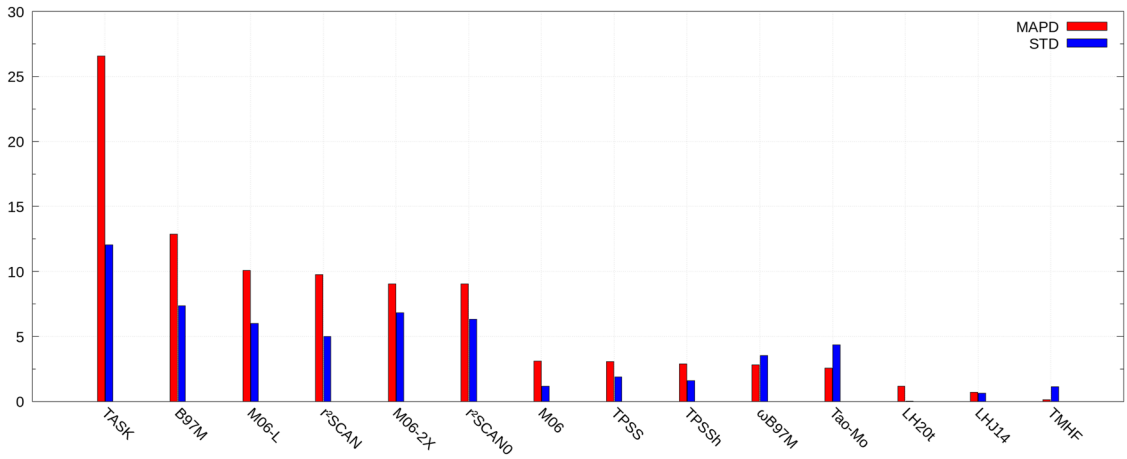

FIG. 4. Impact of the current density on the Δg-shift compared to the parent density functional approximation. MAPD and STD denote the mean absolute percent-wise error and its standard deviation. Shifts below 5 ppt are neglected in the statistical evaluation.

TABLE IV. Impact of the current-dependent generalization of τ on the hyperfine coupling constant of $[TbPc_2]^-$ in MHz (^{159}Tb). Scalar refers to the Fermi-contact and spin-dipole terms in a one-component treatment, SOPT refers to the perturbative treatment of spin–orbit coupling, and 2c SO refers to the self-consistent spin–orbit calculations. Note that the scalar-relativistic calculations are unaffected by the current density. Experimental results are taken from Refs. 207 and 208.

Functional	Scalar	SOPT	2c SO	Functional	Scalar	SOPT	2c SO
Tao-Mo	320.9	542.2	434.0	B97M	728.7	786.8	741.2
cTao-Mo	320.9	574.0	443.3	cB97M	728.7	955.8	801.4
TPSS	189.9	477.8	353.1	ωB97M	235.0	522.7	391.1
cTPSS	189.9	552.8	374.9	cωB97M	235.0	715.8	453.4
TPSSh	154.4	480.6	338.9	LHJ14	50.2	777.2	431.8
cTPSSh	154.4	566.1	367.0	cLHJ14	50.2	548.7	406.3
r^{2}SCAN	519.0	681.9	613.8	TMHF	292.5	739.7	531.6
cr^{2}SCAN	519.0	901.7	678.6	cTMHF	292.5	711.9	526.0
r^{2}SCAN0	362.5	496.7	512.9				
cr^{2}SCAN0	362.5	663.8	606.6				
Expt.	519, 556			Expt.	519, 556		

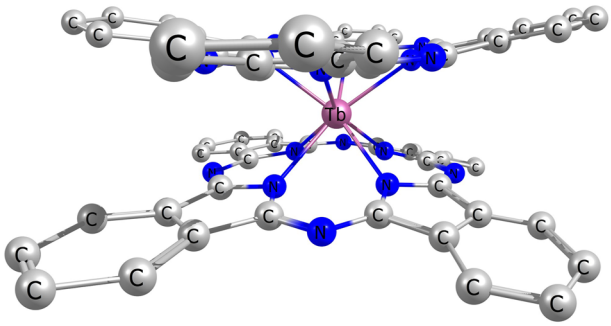

FIG. 5. Molecular structure of $[TbPc_2]^-$ with Pc = bis(phthalocyaninato). H atoms are omitted for clarity. Color code: Tb—purple, N—blue, and C—gray.

the impact of CDFT increases with the importance of the PSO term is further confirmed by studies on lanthanide-based molecules with a doublet ground state and a dominant Fermi-contact interaction in the supplementary material.

Generally, admixture of exact exchange leads to a decrease of the hyperfine coupling constant. In particular, for B97M and ωB97M, the result is almost halved from 741.2 to 391.1 MHz. Among the *meta*-GGAs, the best agreement with the experimental findings is found with the strongly constrained and appropriately normed (SCAN) family, while TPSS and TPSSh substantially underestimate the HFC constant. Overall, TMHF shows the best agreement with the two experimental measurements.

V. CONCLUSION

We have investigated the effects of the paramagnetic current density $\vec{j}_p$ on several properties in the relativistic regime using two-component density functional theory. We find significant effects for semi-local meta-generalized gradient approximation functionals in many properties for open- and closed-shell molecules. The errors of neglecting $\vec{j}_p$ can be vast, leading to severely deteriorated results or even unstable states, as observed, for example, for the excitations of the HfO molecule on several occasions. As argued by Bates and Furche,[95] further neglecting $\vec{j}_p$ will also break the sum rules of TD-DFT in the limit of an infinite basis set. Another known issue is also that iso-orbital indicators may become ill-defined in some systems if $\vec{j}_p$ is neglected. Therefore, we conclude that it is indeed necessary to take into account the current-density dependence for semi-local functionals that depend on the kinetic energy density. Unfortunately, this leads to a significantly raised computational effort that needs to be invested. For example, solving the coupled-perturbed Kohn–Sham equations occurring in the determination of NMR parameters or in time-dependent density functional theory is roughly four times more expensive due to the additional terms that need to be taken into account and the tightened thresholds for the numerical integration.

Overall, the SCAN and Minnesota functional families as well as the B97M and TASK density functional approximations show the largest dependence on the current density. In particular, for TASK, the results are substantially affected by the inclusion of the current density. This may be rationalized by the enhancement factor F_X with respect to the kinetic energy density τ and the constraints introduced in the construction of this functional. Generally, semi-local functionals that aim at recovering charge-transfer (CT) excitations will be notably affected by the current-dependent extension of the kinetic energy density—even for non-CT excited states. Among the studied properties, the largest impact of the current density is observed for EPR g-tensors.

For (local) hybrid functionals, the influence of the paramagnetic current density is less pronounced. However, it can be significant occasionally. For these functionals, the cost of evaluating exact exchange largely outweighs that of the terms arising from $\vec{j}_p$. Additionally, restoring the iso-orbital constraint is of formal importance for local hybrids. Thus, we also recommend to take it into account for the latter class of functionals.

Taking together, the results also indicate that an extension of this work to the gauge-invariant two-component formulation

of NMR shifts and EPR g-tensors is promising for two reasons. First, the current density substantially affects the results already when using a common gauge origin as shown herein. Second, the straightforward generalization of the kinetic energy density with the principle of minimal coupling ensures gauge-origin invariance[209] yet leads to artifacts,[98,99] especially for relativistic calculations and open-shell systems.[98]

SUPPLEMENTARY MATERIAL

The supplementary material is available with the data for the statistical evaluation presented in the main text. Additionally, the X2C theory for NMR shieldings with a common gauge origin is derived. Further studies of NMR and EPR properties to complement the data in the main text are also presented.

ACKNOWLEDGMENTS

C.H. gratefully acknowledges funding from the Volkswagen Foundation. Y.J.F. acknowledges financial support from TURBOMOLE GmbH. Additionally, Y.J.F. is grateful to Fonds der Chemischen Industrie (FCI, German Chemical Industry Funds) for funding of the work on NMR shieldings. A.P. gratefully acknowledges funding from FCI and Studienstiftung des deutschen Volkes.

AUTHOR DECLARATIONS

Conflict of Interest

The authors have no conflicts to disclose.

Author Contributions

C.H. and Y.J.F. contributed equally to this work.

Christof Holzer: Conceptualization (equal); Data curation (equal); Investigation (equal); Methodology (equal); Writing – original draft (equal); Writing – review & editing (equal). **Yannick J. Franzke**: Conceptualization (equal); Data curation (equal); Investigation (equal); Methodology (equal); Writing – original draft (equal); Writing – review & editing (equal). **Ansgar Pausch**: Data curation (supporting); Investigation (supporting); Methodology (supporting); Writing – original draft (supporting); Writing – review & editing (supporting).

DATA AVAILABILITY

The data that support the findings of this study are available within the article and its supplementary material.

APPENDIX: CURRENT-DEPENDENT ATOMIC STATES

Becke outlined in Ref. 66 that neglecting the current density is also the cause of too high energies for atomic states with magnetic quantum numbers M_L when complex spherical harmonic basis functions are used. For real basis functions, which are not eigenfunctions of L_z, we can show that a similar effect can be observed. For each of the p-block atoms B, C, O, and F, two Hartree–Fock, one being a generalized Hartree–Fock (GHF) solution with $L_z = 0$ [which is identical to the unrestricted Hartree-Fock (UHF) solution] and the other one being a GHF solution with $L_z = 1$, are calculated. Then, at each GHF density, simply the energy of the TASK and TPSS functionals and that of their current-dependent version cTASK/cTPSS are calculated non self-consistently. The results, outlined in Table V, clearly show that also in this case, including the paramagnetic current density reduces the gap between these two states significantly, in excellent agreement with the effects observed by Becke.[66]

TABLE V. Total energy differences $E(L_z = 0) - E(L_z = 1)$ for the TASK and current-dependent cTASK functional using the def2-TZVP basis set.[210] All values are in kcal/mol.

Atom	TASK	cTASK	TPSS	cTPSS
B	7.29	−0.13	6.41	4.27
C	8.55	−0.20	5.26	3.75
O	13.16	−0.15	11.56	8.09
F	14.13	0.15	9.19	6.95

For the strongly current-dependent TASK functional, the importance is furthermore considerably higher than for TPSS. Interestingly, cTASK for this specific case outperforms cTPSS. This can be attributed to its stronger current-dependence, but also error cancellation between exchange and correlation may have a positive effect in this case.[66] When spin–orbit coupling is turned on, of course, only M_J is a good quantum number. Given the excellent performance of current-dependent DFT in situations with different M_L, we also expect it to provide significant advantages over standard DFT for treating degeneracies of atomic multiplets with different values of M_J.

REFERENCES

[1] M. Dolg and X. Cao, Chem. Rev. **112**, 403 (2012).
[2] T. Saue, ChemPhysChem **12**, 3077 (2011).
[3] J. Autschbach, J. Chem. Phys. **136**, 150902 (2012).
[4] P. Pyykkö, Annu. Rev. Phys. Chem. **63**, 45 (2012).
[5] K. G. Dyall and K. Fægri, Jr., *Introduction to Relativistic Quantum Chemistry* (Oxford University Press, New York, 2007).
[6] M. Reiher and A. Wolf, *Relativistic Quantum Chemistry: The Fundamental Theory of Molecular Science*, 2nd ed. (Wiley-VCH, Weinheim, Germany, 2015).
[7] *Handbook of Relativistic Quantum Chemistry*, edited by W. Liu (Springer, Berlin, Heidelberg, Germany, 2017).
[8] M. Repisky, S. Komorovsky, R. Bast, and K. Ruud, in *Gas Phase NMR*, edited by K. Jackowski and M. Jaszuński (The Royal Society of Chemistry, Cambridge, UK, 2016), Chap. 8, pp. 267–303.
[9] P. Pyykkö, Chem. Rev. **112**, 371 (2012).
[10] W. Liu, Mol. Phys. **108**, 1679 (2010).
[11] D. Peng and M. Reiher, Theor. Chem. Acc. **131**, 1081 (2012).
[12] T. Nakajima and K. Hirao, Chem. Rev. **112**, 385 (2012).
[13] M. Reiher, Wiley Interdiscip. Rev.: Comput. Mol. Sci. **2**, 139 (2012).
[14] D. Cremer, W. Zou, and M. Filatov, Wiley Interdiscip. Rev.: Comput. Mol. Sci. **4**, 436 (2014).

[15]W. Liu, J. Chem. Phys. **152**, 180901 (2020).
[16]C. Van Wüllen, J. Comput. Chem. **20**, 51 (1999).
[17]C. Van Wüllen, J. Comput. Chem. **23**, 779 (2002).
[18]T. Saue and T. Helgaker, J. Comput. Chem. **23**, 814 (2002).
[19]M. K. Armbruster, F. Weigend, C. van Wüllen, and W. Klopper, Phys. Chem. Chem. Phys. **10**, 1748 (2008).
[20]J. E. Peralta, G. E. Scuseria, and M. J. Frisch, Phys. Rev. B **75**, 125119 (2007).
[21]G. Scalmani and M. J. Frisch, J. Chem. Theory Comput. **8**, 2193 (2012).
[22]F. Wang, T. Ziegler, E. van Lenthe, S. van Gisbergen, and E. J. Baerends, J. Chem. Phys. **122**, 204103 (2005).
[23]J. Gao, W. Zou, W. Liu, Y. Xiao, D. Peng, B. Song, and C. Liu, J. Chem. Phys. **123**, 054102 (2005).
[24]M. Kühn and F. Weigend, J. Chem. Theory Comput. **9**, 5341 (2013).
[25]M. Kühn and F. Weigend, J. Chem. Phys. **142**, 034116 (2015).
[26]A. Baldes and F. Weigend, Mol. Phys. **111**, 2617 (2013).
[27]J. Autschbach, Mol. Phys. **111**, 2544 (2013).
[28]M. Kehry, Y. J. Franzke, C. Holzer, and W. Klopper, Mol. Phys. **118**, e1755064 (2020).
[29]F. Egidi, S. Sun, J. J. Goings, G. Scalmani, M. J. Frisch, and X. Li, J. Chem. Theory Comput. **13**, 2591 (2017).
[30]W. Liu and Y. Xiao, Chem. Soc. Rev. **47**, 4481 (2018).
[31]S. Komorovsky, P. J. Cherry, and M. Repisky, J. Chem. Phys. **151**, 184111 (2019).
[32]J. K. Desmarais, S. Komorovsky, J.-P. Flament, and A. Erba, J. Chem. Phys. **154**, 204110 (2021).
[33]M. Mayer, O. D. Häberlen, and N. Rösch, Phys. Rev. A **54**, 4775 (1996).
[34]S. Varga, E. Engel, W.-D. Sepp, and B. Fricke, Phys. Rev. A **59**, 4288 (1999).
[35]W. Liu and C. van Wüllen, J. Chem. Phys. **110**, 3730 (1999).
[36]W. Liu and C. van Wüllen, J. Chem. Phys. **113**, 891 (2000).
[37]S. Varga, B. Fricke, H. Nakamatsu, T. Mukoyama, J. Anton, D. Geschke, A. Heitmann, E. Engel, and T. Baştuğ, J. Chem. Phys. **112**, 3499 (2000).
[38]W. Liu and C. van Wüllen, J. Chem. Phys. **113**, 2506 (2000).
[39]M. Repisky, S. Komorovsky, M. Kadek, L. Konecny, U. Ekström, E. Malkin, M. Kaupp, K. Ruud, O. L. Malkina, and V. G. Malkin, J. Chem. Phys. **152**, 184101 (2020).
[40]Y. Zhang, B. Suo, Z. Wang, N. Zhang, Z. Li, Y. Lei, W. Zou, J. Gao, D. Peng, Z. Pu, Y. Xiao, Q. Sun, F. Wang, Y. Ma, X. Wang, Y. Guo, and W. Liu, J. Chem. Phys. **152**, 064113 (2020).
[41]T. Saue, R. Bast, A. S. P. Gomes, H. J. A. Jensen, L. Visscher, I. A. Aucar, R. Di Remigio, K. G. Dyall, E. Eliav, E. Fasshauer, T. Fleig, L. Halbert, E. D. Hedegård, B. Helmich-Paris, M. Iliaš, C. R. Jacob, S. Knecht, J. K. Laerdahl, M. L. Vidal, M. K. Nayak, M. Olejniczak, J. M. H. Olsen, M. Pernpointner, B. Senjean, A. Shee, A. Sunaga, and J. N. P. van Stralen, J. Chem. Phys. **152**, 204104 (2020).
[42]D. B. Williams-Young, A. Petrone, S. Sun, T. F. Stetina, P. Lestrange, C. E. Hoyer, D. R. Nascimento, L. Koulias, A. Wildman, J. Kasper, J. J. Goings, F. Ding, A. E. DePrince III, E. F. Valeev, and X. Li, Wiley Interdiscip. Rev.: Comput. Mol. Sci. **10**, e1436 (2020).
[43]E. Aprà, E. J. Bylaska, W. A. de Jong, N. Govind, K. Kowalski, T. P. Straatsma, M. Valiev, H. J. J. van Dam, Y. Alexeev, J. Anchell, V. Anisimov, F. W. Aquino, R. Atta-Fynn, J. Autschbach, N. P. Bauman, J. C. Becca, D. E. Bernholdt, K. Bhaskaran-Nair, S. Bogatko, P. Borowski, J. Boschen, J. Brabec, A. Bruner, E. Cauët, Y. Chen, G. N. Chuev, C. J. Cramer, J. Daily, M. J. O. Deegan, T. H. Dunning, M. Dupuis, K. G. Dyall, G. I. Fann, S. A. Fischer, A. Fonari, H. Früchtl, L. Gagliardi, J. Garza, N. Gawande, S. Ghosh, K. Glaesemann, A. W. Götz, J. Hammond, V. Helms, E. D. Hermes, K. Hirao, S. Hirata, M. Jacquelin, L. Jensen, B. G. Johnson, H. Jónsson, R. A. Kendall, M. Klemm, R. Kobayashi, V. Konkov, S. Krishnamoorthy, M. Krishnan, Z. Lin, R. D. Lins, R. J. Littlefield, A. J. Logsdail, K. Lopata, W. Ma, A. V. Marenich, J. Martin del Campo, D. Mejia-Rodriguez, J. E. Moore, J. M. Mullin, T. Nakajima, D. R. Nascimento, J. A. Nichols, P. J. Nichols, J. Nieplocha, A. Otero-de-la-Roza, B. Palmer, A. Panyala, T. Pirojsirikul, B. Peng, R. Peverati, J. Pittner, L. Pollack, R. M. Richard, P. Sadayappan, G. C. Schatz, W. A. Shelton, D. W. Silverstein, D. M. A. Smith, T. A. Soares, D. Song, M. Swart, H. L. Taylor, G. S. Thomas, V. Tipparaju, D. G. Truhlar, K. Tsemekhman, T. Van Voorhis, Á. Vázquez-Mayagoitia, P. Verma, O. Villa, A. Vishnu, K. D. Vogiatzis, D. Wang, J. H. Weare, M. J. Williamson, T. L. Windus, K. Woliński, A. T. Wong, Q. Wu, C. Yang, Q. Yu, M. Zacharias, Z. Zhang, Y. Zhao, and R. J. Harrison, J. Chem. Phys. **152**, 184102 (2020).
[44]G. te Velde, F. M. Bickelhaupt, E. J. Baerends, C. Fonseca Guerra, S. J. A. van Gisbergen, J. G. Snijders, and T. Ziegler, J. Comput. Chem. **22**, 931 (2001).
[45]M. Hayami, J. Seino, Y. Nakajima, M. Nakano, Y. Ikabata, T. Yoshikawa, T. Oyama, K. Hiraga, S. Hirata, and H. Nakai, J. Comput. Chem. **39**, 2333 (2018).
[46]L. Belpassi, M. De Santis, H. M. Quiney, F. Tarantelli, and L. Storchi, J. Chem. Phys. **152**, 164118 (2020).
[47]S. G. Balasubramani, G. P. Chen, S. Coriani, M. Diedenhofen, M. S. Frank, Y. J. Franzke, F. Furche, R. Grotjahn, M. E. Harding, C. Hättig, A. Hellweg, B. Helmich-Paris, C. Holzer, U. Huniar, M. Kaupp, A. Marefat Khah, S. Karbalaei Khani, T. Müller, F. Mack, B. D. Nguyen, S. M. Parker, E. Perlt, D. Rappoport, K. Reiter, S. Roy, M. Rückert, G. Schmitz, M. Sierka, E. Tapavicza, D. P. Tew, C. van Wüllen, V. K. Voora, F. Weigend, A. Wodyński, and J. M. Yu, J. Chem. Phys. **152**, 184107 (2020).
[48]J. Jaramillo, G. E. Scuseria, and M. Ernzerhof, J. Chem. Phys. **118**, 1068 (2003).
[49]T. M. Maier, A. V. Arbuznikov, and M. Kaupp, Wiley Interdiscip. Rev.: Comput. Mol. Sci. **9**, e1378 (2018).
[50]E. R. Johnson, J. Chem. Phys. **141**, 124120 (2014).
[51]J. P. Perdew, V. N. Staroverov, J. Tao, and G. E. Scuseria, Phys. Rev. A **78**, 052513 (2008).
[52]M. Haasler, T. M. Maier, R. Grotjahn, S. Gückel, A. V. Arbuznikov, and M. Kaupp, J. Chem. Theory Comput. **16**, 5645 (2020).
[53]C. Holzer and Y. J. Franzke, J. Chem. Phys. **157**, 034108 (2022).
[54]T. Saue, "Spin-interactions and the non-relativistic limit of electrodynamics," in *Advances in Quantum Chemistry*, edited by J. R. Sabin, E. Brändas, and L. B. Oddershede (Elsevier Academic Press, San Diego, CA, 2005), Vol. 48, pp. 383–405.
[55]J. K. Desmarais, J.-P. Flament, and A. Erba, Phys. Rev. B **101**, 235142 (2020).
[56]R. E. Moss, *Advanced Molecular Quantum Mechanics: An Introduction to Relativistic Quantum Mechanics and the Quantum Theory of Radiation* (Chapman & Hall, London, UK, 1973), pp. 81–84.
[57]P. Atkins and R. Friedman, *Molecular Quantum Mechanics*, 5th ed. (Oxford University Press, New York, 2010), pp. 215–217.
[58]A. Pausch and C. Holzer, J. Chem. Phys. Lett. **13**, 4335 (2022).
[59]J. K. Desmarais, J.-P. Flament, and A. Erba, Phys. Rev. B **102**, 235118 (2020).
[60]J. Tao and J. P. Perdew, Phys. Rev. Lett. **95**, 196403 (2005).
[61]S. Pittalis, S. Kurth, S. Sharma, and E. K. U. Gross, J. Chem. Phys. **127**, 124103 (2007).
[62]E. Räsänen, S. Pittalis, and C. R. Proetto, J. Chem. Phys. **132**, 044112 (2010).
[63]S. Pittalis, E. Räsänen, and E. K. U. Gross, Phys. Rev. A **80**, 032515 (2009).
[64]F. Bodo, J. K. Desmarais, and A. Erba, Phys. Rev. B **105**, 125108 (2022).
[65]J. F. Dobson, J. Chem. Phys. **98**, 8870 (1993).
[66]A. D. Becke, J. Chem. Phys. **117**, 6935 (2002).
[67]J. Tao, Phys. Rev. B **71**, 205107 (2005).
[68]T. Burnus, M. A. L. Marques, and E. K. U. Gross, Phys. Rev. A **71**, 010501 (2005).
[69]G. Vignale and M. Rasolt, Phys. Rev. B **37**, 10685 (1988).
[70]G. Vignale and M. Rasolt, Phys. Rev. B **39**, 5475 (1989).
[71]A. Laestadius, Int. J. Quantum Chem. **114**, 1445 (2014).
[72]A. Laestadius and M. Benedicks, Int. J. Quantum Chem. **114**, 782 (2014).
[73]A. Laestadius, J. Math. Chem. **52**, 2581 (2014).
[74]A. Laestadius and M. Benedicks, Phys. Rev. A **91**, 032508 (2015).
[75]E. I. Tellgren, S. Kvaal, E. Sagvolden, U. Ekström, A. M. Teale, and T. Helgaker, Phys. Rev. A **86**, 062506 (2012).
[76]E. I. Tellgren, A. M. Teale, J. W. Furness, K. K. Lange, U. Ekström, and T. Helgaker, J. Chem. Phys. **140**, 034101 (2014).
[77]E. I. Tellgren, S. Kvaal, and T. Helgaker, Phys. Rev. A **89**, 012515 (2014).
[78]E. H. Lieb and R. Schrader, Phys. Rev. A **88**, 032516 (2013).
[79]S. Reimann, U. Ekström, S. Stopkowicz, A. M. Teale, A. Borgoo, and T. Helgaker, Phys. Chem. Chem. Phys. **17**, 18834 (2015).
[80]J. W. Furness, J. Verbeke, E. I. Tellgren, S. Stopkowicz, U. Ekström, T. Helgaker, and A. M. Teale, J. Chem. Theory Comput. **11**, 4169 (2015).
[81]T. J. P. Irons, L. Spence, G. David, B. T. Speake, T. Helgaker, and A. M. Teale, J. Phys. Chem. A **124**, 1321 (2020).
[82]S. Sen and E. I. Tellgren, J. Chem. Theory Comput. **17**, 1480 (2021).

[83]T. J. P. Irons, G. David, and A. M. Teale, J. Chem. Theory Comput. **17**, 2166 (2021).
[84]K. G. Dyall, J. Chem. Phys. **106**, 9618 (1997).
[85]K. G. Dyall, J. Chem. Phys. **109**, 4201 (1998).
[86]K. G. Dyall and T. Enevoldsen, J. Chem. Phys. **111**, 10000 (1999).
[87]K. G. Dyall, J. Chem. Phys. **115**, 9136 (2001).
[88]W. Kutzelnigg and W. Liu, J. Chem. Phys. **123**, 241102 (2005).
[89]W. Liu and W. Kutzelnigg, J. Chem. Phys. **126**, 114107 (2007).
[90]W. Liu and D. Peng, J. Chem. Phys. **125**, 044102 (2006).
[91]W. Liu and D. Peng, J. Chem. Phys. **125**, 149901 (2006).
[92]M. Iliaš and T. Saue, J. Chem. Phys. **126**, 064102 (2007).
[93]W. Liu and D. Peng, J. Chem. Phys. **131**, 031104 (2009).
[94]D. Peng, W. Liu, Y. Xiao, and L. Cheng, J. Chem. Phys. **127**, 104106 (2007).
[95]J. E. Bates and F. Furche, J. Chem. Phys. **137**, 164105 (2012).
[96]J. Liang, X. Feng, D. Hait, and M. Head-Gordon, J. Chem. Theory Comput. **18**, 3460 (2022).
[97]F. Bruder, Y. J. Franzke, and F. Weigend, J. Phys. Chem. A **126**, 5050 (2022).
[98]Y. J. Franzke and C. Holzer, J. Chem. Phys. **157**, 031102 (2022).
[99]C. J. Schattenberg and M. Kaupp, J. Chem. Theory Comput. **17**, 1469 (2021).
[100]C. Holzer, Y. J. Franzke, and M. Kehry, J. Chem. Theory Comput. **17**, 2928 (2021).
[101]Y. J. Franzke, F. Mack, and F. Weigend, J. Chem. Theory Comput. **17**, 3974 (2021).
[102]Y. J. Franzke, C. Holzer, and F. Mack, J. Chem. Theory Comput. **18**, 1030 (2022).
[103]J. A. Pople, P. M. W. Gill, and B. G. Johnson, Chem. Phys. Lett. **199**, 557 (1992).
[104]F. London, J. Phys. Radium **8**, 397 (1937).
[105]R. Ditchfield, Mol. Phys. **27**, 789 (1974).
[106]A. D. Becke, J. Chem. Phys. **88**, 2547 (1988).
[107]C. W. Murray, N. C. Handy, and G. J. Laming, Mol. Phys. **78**, 997 (1993).
[108]P. M. W. Gill, B. G. Johnson, and J. A. Pople, Chem. Phys. Lett. **209**, 506 (1993).
[109]O. Treutler and R. Ahlrichs, J. Chem. Phys. **102**, 346 (1995).
[110]A. V. Arbuznikov and M. Kaupp, J. Chem. Phys. **141**, 204101 (2014).
[111]T. M. Maier, M. Haasler, A. V. Arbuznikov, and M. Kaupp, Phys. Chem. Chem. Phys. **18**, 21133 (2016).
[112]P. Plessow and F. Weigend, J. Comput. Chem. **33**, 810 (2012).
[113]C. Holzer, J. Chem. Phys. **153**, 184115 (2020).
[114]H. Bahmann and M. Kaupp, J. Chem. Theory Comput. **11**, 1540 (2015).
[115]I. Malkin, O. L. Malkina, V. G. Malkin, and M. Kaupp, J. Chem. Phys. **123**, 244103 (2005).
[116]E. Malkin, M. Repiský, S. Komorovský, P. Mach, O. L. Malkina, and V. G. Malkin, J. Chem. Phys. **134**, 044111 (2011).
[117]S. Gohr, P. Hrobárik, M. Repiský, S. Komorovský, K. Ruud, and M. Kaupp, J. Phys. Chem. A **119**, 12892 (2015).
[118]A. Wodyński and M. Kaupp, J. Chem. Theory Comput. **16**, 314 (2020).
[119]Y. J. Franzke and J. M. Yu, J. Chem. Theory Comput. **18**, 323 (2022).
[120]Y. J. Franzke and J. M. Yu, J. Chem. Theory Comput. **18**, 2246 (2022).
[121]J. Autschbach, D. Peng, and M. Reiher, J. Chem. Theory Comput. **8**, 4239 (2012).
[122]P. Verma and J. Autschbach, J. Chem. Theory Comput. **9**, 1052 (2013).
[123]M. Glasbrenner, S. Vogler, and C. Ochsenfeld, J. Chem. Phys. **148**, 214101 (2018).
[124]C. Holzer and W. Klopper, J. Chem. Phys. **150**, 204116 (2019).
[125]H. Bahmann, A. Rodenberg, A. V. Arbuznikov, and M. Kaupp, J. Chem. Phys. **126**, 011103 (2007).
[126]A. V. Arbuznikov and M. Kaupp, Chem. Phys. Lett. **440**, 160 (2007).
[127]A. V. Arbuznikov and M. Kaupp, J. Chem. Phys. **136**, 014111 (2012).
[128]R. Ahlrichs, M. Bär, M. Häser, H. Horn, and C. Kölmel, Chem. Phys. Lett. **162**, 165 (1989).
[129]F. Furche, R. Ahlrichs, C. Hättig, W. Klopper, M. Sierka, and F. Weigend, Wiley Interdiscip. Rev.: Comput. Mol. Sci. **4**, 91 (2014).
[130]Developers' version of TURBOMOLE V7.6 2021, a development of University of Karlsruhe and Forschungszentrum Karlsruhe GmbH, 1989–2007, TURBOMOLE GmbH, since 2007; available from https://www.turbomole.org, retrieved January 12, 2022.
[131]A. Pausch and W. Klopper, Mol. Phys. **118**, e1736675 (2020).
[132]C. Holzer, A. Pausch, and W. Klopper, Front. Chem. **9**, 746162 (2021).
[133]A. Pausch, C. Holzer, and W. Klopper, J. Chem. Theory Comput. **18**, 3747 (2022).
[134]M. A. L. Marques, M. J. T. Oliveira, and T. Burnus, Comput. Phys. Commun. **183**, 2272 (2012).
[135]S. Lehtola, C. Steigemann, M. J. T. Oliveira, and M. A. L. Marques, SoftwareX **7**, 1 (2018).
[136]Libxc, version 5.1.7 and version 5.2.3, available from https://www.tddft.org/programs/libxc/, retrieved August 16, 2022.
[137]U. Ekström, L. Visscher, R. Bast, A. J. Thorvaldsen, and K. Ruud, J. Chem. Theory Comput. **6**, 1971 (2010).
[138]OpenMP architecture review boards, OpenMP API shared-memory parallel programming, https://www.openmp.org, retrieved September 26, 2021.
[139]C. Holzer and Y. J. Franzke, OpenMP version of ridft, rdgrad, and egrad with contributions to mpshift, dscf, and grad; improved OpenMP version of aoforce and escf, released with TURBOMOLE V7.4 and further improved in TURBOMOLE V7.5.
[140]O. Treutler, "Entwicklung und anwendung von dichtefunktionalmethoden," Ph.D. dissertation [University of Karlsruhe (TH), Germany, 1995].
[141]Y. J. Franzke, N. Middendorf, and F. Weigend, J. Chem. Phys. **148**, 104110 (2018).
[142]C. Holzer and W. Klopper, J. Chem. Phys. **149**, 101101 (2018).
[143]S. Komorovský, M. Repiský, O. L. Malkina, V. G. Malkin, I. Malkin Ondík, and M. Kaupp, J. Chem. Phys. **128**, 104101 (2008).
[144]R. Kelting, A. Baldes, U. Schwarz, T. Rapps, D. Schooss, P. Weis, C. Neiss, F. Weigend, and M. M. Kappes, J. Chem. Phys. **136**, 154309 (2012).
[145]B. Metz, H. Stoll, and M. Dolg, J. Chem. Phys. **113**, 2563 (2000).
[146]J. Tao, J. P. Perdew, V. N. Staroverov, and G. E. Scuseria, Phys. Rev. Lett. **91**, 146401 (2003).
[147]F. Weigend and A. Baldes, J. Chem. Phys. **133**, 174102 (2010).
[148]K. Eichkorn, O. Treutler, H. Öhm, M. Häser, and R. Ahlrichs, Chem. Phys. Lett. **240**, 283 (1995).
[149]K. Eichkorn, F. Weigend, O. Treutler, and R. Ahlrichs, Theor. Chem. Acc. **97**, 119 (1997).
[150]F. Weigend, M. Kattannek, and R. Ahlrichs, J. Chem. Phys. **130**, 164106 (2009).
[151]F. Weigend, Phys. Chem. Chem. Phys. **8**, 1057 (2006).
[152]T. Aschebrock and S. Kümmel, Phys. Rev. Res. **1**, 033082 (2019).
[153]P. Tecmer, R. Bast, K. Ruud, and L. Visscher, J. Chem. Phys. A **116**, 7397 (2012).
[154]D. Ravelli, D. Dondi, M. Fagnoni, A. Albini, and A. Bagno, J. Comput. Chem. **32**, 2983 (2011).
[155]D. Peng, N. Middendorf, F. Weigend, and M. Reiher, J. Chem. Phys. **138**, 184105 (2013).
[156]P. Pollak and F. Weigend, J. Chem. Theory Comput. **13**, 3696 (2017).
[157]Y. J. Franzke, L. Spiske, P. Pollak, and F. Weigend, J. Chem. Theory Comput. **16**, 5658 (2020).
[158]K. A. Peterson, J. Chem. Phys. **142**, 074105 (2015).
[159]J. Tao and Y. Mo, Phys. Rev. Lett. **117**, 073001 (2016).
[160]V. N. Staroverov, G. E. Scuseria, J. Tao, and J. P. Perdew, J. Chem. Phys. **119**, 12129 (2003).
[161]J. W. Furness, A. D. Kaplan, J. Ning, J. P. Perdew, and J. Sun, J. Phys. Chem. Lett. **11**, 8208 (2020).
[162]J. W. Furness, A. D. Kaplan, J. Ning, J. P. Perdew, and J. Sun, J. Phys. Chem. Lett. **11**, 9248 (2020).
[163]M. Bursch, H. Neugebauer, S. Ehlert, and S. Grimme, J. Chem. Phys. **156**, 134105 (2022).
[164]N. Mardirossian and M. Head-Gordon, J. Chem. Phys. **142**, 074111 (2015).
[165]N. Mardirossian and M. Head-Gordon, J. Chem. Phys. **144**, 214110 (2016).
[166]Y. Zhao and D. G. Truhlar, J. Chem. Phys. **125**, 194101 (2006).

[167]Y. Zhao and D. G. Truhlar, Theor. Chem. Acc. **120**, 215 (2008).
[168]Y. J. Franzke, R. Treß, T. M. Pazdera, and F. Weigend, Phys. Chem. Chem. Phys. **21**, 16658 (2019).
[169]R. E. Stanton and S. Havriliak, J. Chem. Phys. **81**, 1910 (1984).
[170]J. C. Boettger, Phys. Rev. B **62**, 7809 (2000).
[171]M. Filatov, W. Zou, and D. Cremer, J. Chem. Phys. **139**, 014106 (2013).
[172]W. Zou, M. Filatov, and D. Cremer, J. Chem. Phys. **142**, 214106 (2015).
[173]T. Yoshizawa, W. Zou, and D. Cremer, J. Chem. Phys. **145**, 184104 (2016).
[174]L. Visscher and K. G. Dyall, At. Data Nucl. Data Tables **67**, 207 (1997).
[175]K. P. Huber and G. H. Herzberg, *Constants of Diatomic Molecules* (Van Nostrand Reinhold, New York, 1979), see also https://webbook.nist.gov/, retrieved August 1, 2022.
[176]J. Styszyński, Chem. Phys. Lett. **317**, 351 (2000).
[177]M. Balmer, Y. J. Franzke, F. Weigend, and C. Hänisch, Chem. - Eur. J. **26**, 192 (2020).
[178]Y. J. Franzke and F. Weigend, J. Chem. Theory Comput. **15**, 1028 (2019).
[179]S. Gillhuber, Y. J. Franzke, and F. Weigend, J. Phys. Chem. A **125**, 9707 (2021).
[180]A. R. Eulenstein, Y. J. Franzke, P. Bügel, W. Massa, F. Weigend, and S. Dehnen, Nat. Commun. **11**, 5122 (2020).
[181]A. R. Eulenstein, Y. J. Franzke, N. Lichtenberger, R. J. Wilson, H. L. Deubner, F. Kraus, R. Clérac, F. Weigend, and S. Dehnen, Nat. Chem. **13**, 149 (2021).
[182]A. Klamt and G. Schüürmann, J. Chem. Soc., Perkin Trans. 2 **1993**, 799.
[183]A. Schäfer, A. Klamt, D. Sattel, J. C. W. Lohrenz, and F. Eckert, Phys. Chem. Chem. Phys. **2**, 2187 (2000).
[184]A. L. Wysocki and K. Park, Inorg. Chem. **59**, 2771 (2020).
[185]F. Branzoli, P. Carretta, M. Filibian, G. Zoppellaro, M. J. Graf, J. R. Galan-Mascaros, O. Fuhr, S. Brink, and M. Ruben, J. Am. Chem. Soc. **131**, 4387 (2009).
[186]K. Kundu, J. R. K. White, S. A. Moehring, J. M. Yu, J. W. Ziller, F. Furche, W. J. Evans, and S. Hill, Nat. Chem. **14**, 392 (2022).
[187]S. M. Bass, R. L. DeLeon, and J. S. Muenter, J. Chem. Phys. **86**, 4305 (1987).
[188]W. G. Schneider, H. J. Bernstein, and J. A. Pople, J. Chem. Phys. **28**, 601 (1958).
[189]D. K. Hindermann and C. D. Cornwell, J. Chem. Phys. **48**, 2017 (1968).
[190]W. T. Rayes, in *Nuclear Magnetic Resonance*, Specialist Periodical Report Vol. 7, edited by R. J. Abraham (The Royal Society of Chemisty, Oxford, UK, 1978), Chap. 1, pp. 1–25.
[191]M. Olejniczak, R. Bast, T. Saue, and M. Pecul, J. Chem. Phys. **136**, 014108 (2012).
[192]J. Schmitte, C. Friebel, F. Weller, and K. Dehnicke, Z. Anorg. Allg. Chem. **495**, 148 (1982).
[193]K. K. Sunil and M. T. Rogers, Inorg. Chem. **20**, 3283 (1981).
[194]P. T. Manoharan and M. T. Rogers, J. Chem. Phys. **49**, 5510 (1968).
[195]J. T. C. van Kemenade, "Ligand hyperfine interactions in oxyhalides of pentavalent chromium, molybdenum and tungsten," Ph.D. thesis, Technical University Delft, The Netherlands, 1970.
[196]J. Baldas, J. Boas, and J. Bonnyman, Aust. J. Chem. **42**, 639 (1989).
[197]J. Baldas, J. F. Boas, J. Bonnyman, and G. A. Williams, J. Chem. Soc., Dalton Trans. **1984**, 2395.
[198]M. Kersting, C. Friebel, K. Dehnicke, M. Krestel, and R. Allmann, Z. Anorg. Allg. Chem. **563**, 70 (1988).
[199]A. Voigt, U. Abram, and R. Kirmse, Inorg. Chem. Commun. **1**, 141 (1998).
[200]A. Voigt, U. Abram, R. Böttcher, U. Richter, J. Reinhold, and R. Kirmse, Chem. Phys. **253**, 171 (2000).
[201]U. Abram, M. Braun, S. Abram, R. Kirmse, and A. Voigt, J. Chem. Soc., Dalton Trans. **1998**, 231.
[202]L. V. Borisova, A. N. Ermakov, Y. I. Plastinina, O. D. Prasolova, and I. N. Marov, Analyst **107**, 500 (1982).
[203]J. H. Holloway, E. G. Hope, J. B. Raynor, and P. T. Townson, J. Chem. Soc., Dalton Trans. **1992**, 1131.
[204]J. Autschbach and B. Pritchard, Theor. Chem. Acc. **129**, 453 (2011).
[205]G. Schreckenbach and T. Ziegler, J. Phys. Chem. A **101**, 3388 (1997).
[206]G. Schreckenbach and T. Ziegler, Theor. Chem. Acc. **99**, 71 (1998).
[207]N. Ishikawa, M. Sugita, and W. Wernsdorfer, Angew. Chem., Int. Ed. **44**, 2931 (2005).
[208]G. Taran, E. Bonet, and W. Wernsdorfer, J. Appl. Phys. **125**, 142903 (2019).
[209]S. N. Maximoff and G. E. Scuseria, Chem. Phys. Lett. **390**, 408 (2004).
[210]F. Weigend and R. Ahlrichs, Phys. Chem. Chem. Phys. **7**, 3297 (2005).